Review
doi.org/10.1002/elsa.202300014

Chemistry Europe
European Chemical Societies Publishing

Received: 1 May 2023
Revised: 30 June 2023
Accepted: 8 July 2023

Probing passivity of corroding metals using scanning electrochemical probe microscopy

Sebastian Amland Skaanvik[1] | **Samantha Michelle Gateman**[2,3]

[1]Interdisciplinary Nanoscience Center, Aarhus University, Aarhus, Denmark

[2]Department of Chemistry, Western University, London, Ontario, Canada

[3]Surface Science Western, Western University, London, Ontario, Canada

Correspondence
Samantha Michelle Gateman, Western University, 1151 Richmond Street, London, Ontario, Canada, N6A 5B7.
Email: samantha.gateman@uwo.ca

Funding information
Natural Sciences and Engineering Research Council of Canada, Grant/Award Number: RGPIN-2022-04696

Abstract

Passive films are essential for the longevity of metals and alloys in corrosive environments. A great deal of research has been devoted to understanding and characterizing passive films, including their chemical composition, uniformity, thickness, porosity, and conductivity. Many characterization techniques are conducted under vacuum, which do not portray the true in-service environments passive films will endure. Scanning electrochemical probe microscopy (SEPM) techniques have emerged as necessary tools to complement research on characterizing passive films to enable the in situ extraction of passive film parameters and monitoring of local breakdown events of compromised films. Herein, we review the current research efforts using scanning electrochemical microscopy, scanning electrochemical cell microscopy (or droplet cell measurements), and local electrochemical impedance spectroscopy techniques to advance the knowledge of local properties of passivated metals. The future use of SEPM for quantitative extraction of local film characteristics within in-service environments (i.e., with varying pH, solution composition, and applied potential) is promising, which can be correlated to nanostructural and microstructural features of the passive film and underlying metal using complementary microscopy and spectroscopy methods. The outlook on this topic is highlighted, including exciting avenues and challenges of these methods in characterizing advanced alloy systems and protective surface films.

Abbreviations: SEPM, scanning electrochemical probe microscopy; EDX, energy-dispersive X-ray spectroscopy; XPS, X-ray photoelectron spectroscopy; AES, Auger electron spectroscopy; EIS, electrochemical impedance spectroscopy; EC-STM, electrochemical scanning tunneling microscopy; EC-AFM, electrochemical atomic force microscopy; SVET, scanning vibrating electrode technique; LEIS, local electrochemical impedance spectroscopy; SKP, scanning Kelvin probe; KPFM, Kelvin probe force microscopy; SECM, scanning electrochemical microscopy; SECCM, scanning electrochemical cell microscopy; EDC, electrochemical droplet cell; AC, alternating current; SICM, scanning ion conductance microscopy; UME, ultra-microelectrode; WE, working electrode; RE, reference electrode; CE, counter electrode; G/C, generation/collection; SG/TC, substrate generation/tip collection; TG/SC, tip generation/substrate collection; AC-SECM, alternating-current scanning electrochemical microscopy; DC, direct current; SMCM, scanning micropipette contact method; SEM, scanning electron microscopy; AFM, atomic force microscopy; EBSD, electron backscatter diffraction; Micro-PDP, micro-potentiodynamic polarization; TOF-SIMS, time-of-flight secondary ion mass spectrometry; SCE, saturated calomel electrode; STM, scanning tunneling microscopy; C-AFM, conductive atomic force microscopy; OCP, open circuit potential; PDP, potentiodynamic polarization; HER, hydrogen evolution reaction; HEAs, high entropy alloys; PDM, point defect model.

Review
doi.org/10.1002/elsa.202300014
Chemistry Europe
European Chemical Societies Publishing

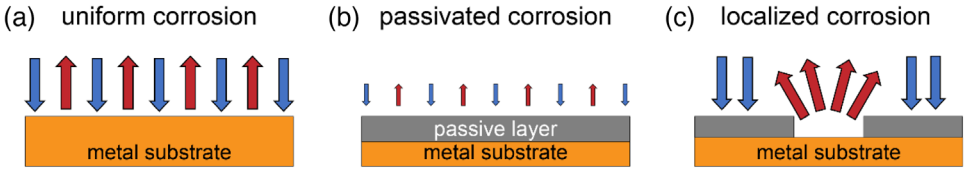

FIGURE 1 Schematic representation of different corrosion states dependent on the distribution of cathodic and anodic processes. Blue and red arrows indicate mass-transport of cathodic (oxidant, e.g., O_2 and H_2O) and anodic species (primarily metal cations), respectively. Panel (a) describes uniform corrosion where the cathodic and anodic processes are uniformly distributed across the corroding metal surface. Panel (b) shows a passivated metal where the rate-limiting reactions are reduced. Panel (c) demonstrates localized corrosion, where the anodic and cathodic processes are locally distributed, arising from local passive film breakdown.

1 | INTRODUCTION TO PASSIVITY

Over the past two centuries, there has been a great deal of research dedicated to understanding surface passivation and its role in many electrochemical systems including corroding metals,[1] electrochemical water splitting,[2,3] fuel cell performance,[4,5] and solid electrolyte interfaces in energy storage systems.[6,7] Among the systems influenced, passivation in corrosion science is of historical importance.[8] It was the work done by Schönbein and Faraday in 1836 that ignited the term "passivation" to describe the observation of the protective oxide layer that forms on iron preferentially in highly concentrated nitric acid.[9] Still today, the study of passive corroding systems remains at the forefront of research efforts and a central issue in corrosion science and engineering.[8,10]

Corrosion is a thermodynamically favorable process that costs the world 3.4% of its global domestic product.[11] The safety concerns, environmental impact, and economic waste produced by metal corrosion make understanding this degradation a priority in many industry-relevant scenarios. The electrochemical process of active corrosion involves the simultaneous transfer of mass and charge across a solid–liquid interface, where metal oxidation produces metal ions that move into the bulk solution (Figure 1a). A passivated metal holds the ability to resist active corrosion due to the spontaneous formation of a thin, dense, and well-adhered passive film that limits and electrochemical activity of a metal's surface (Figure 1b).[12] This is accomplished by slowing the diffusion of oxidizing agents (e.g., oxygen) to the metal's surface and/or metal ions from the surface through the creation of a steep concentration gradient adjacent to the metal.[13] When the passive film is locally compromised, the exposure of the underlying metal can result in the highly localized distribution of anodic and/or cathodic sites and rapid local metal dissolution, known as localized corrosion (Figure 1c).

Passivation can occur spontaneously in air through rapid oxidation or precipitation from an anodic process in solution.[14] Metals and their alloys that have demonstrated passive behavior include (but are not limited to) Ni,[15] Cr,[16] Fe,[17] Cu,[18] Al,[19] Ti,[20] and Zr.[21] Among passivated alloys, the protectiveness of the Cr-rich protective oxide film formed on stainless steels (i.e., ferrous alloys) has been extensively studied.[22,23] This definition of passivation excludes protective films composed of other materials, such as inhibitors[24,25] or organic-based coatings,[26,27] which aim to hold the same functionality as spontaneous or anodically grown passive films.[28] The chemical composition of a passive film typically consists of precipitated metal ions with components from the adjacent environment, mainly oxygen and/or water, to form metal oxides and/or hydroxides.[8] Several oxidation states of the metal cation can be present, and in the case of alloyed systems, the passive film may consist of one or more metallic components. Due to the thin nature of passive films, their chemical composition and thickness values were previously difficult to measure with confidence.[12] The development of aberration-corrected scanning transmission electron microscopy coupled with energy-dispersive X-ray spectroscopy (EDX) has enabled sub-nm investigations of cross-sectioned passive films for direct observation of film thickness and chemical composition.[29–31] Advancement in and utilization of surface analysis tools such as X-ray photoelectron spectroscopy (XPS),[32] Auger electron spectroscopy (AES),[33] ion scattering spectroscopy,[34] and Rutherford backscattering spectrometry[35,36] has enabled the characterization of the chemical composition and film thickness of passive films and has revealed a bilayer or multilayer structure typically consisting of a compact, inner oxide layer and a hydrated surface film for many passivating systems.[1,37]

Macroscale electrochemical methods are routinely used to classify a material as "passive" and have been utilized to provide dynamic information on the properties of protective oxide films. Unlike surface analysis tools that require ultra-high vacuum conditions and result in X-ray-generated heat, the advantage of using electrochemical methods is the direct study of immersed and hydrated passive metals while under in-service conditions. For instance, electrochemical impedance spectroscopy (EIS) has been used to extract resistivity profiles and passive film thicknesses.[38] Voltammetry measurements portray

doi.org/10.1002/elsa.202300014

a metal's ability to form a protective passive layer by the observation of a steep decrease in anodic current density that becomes independent of applied potential (diffusion limited) within a specific potential window.[39] The potential at which a sharp increase in current density is observed, called the breakdown potential, signifies the formation of localized corrosion (i.e., pitting). Monitoring a material's hysteresis behavior during cyclic voltammetry can elucidate information about the material's self-healing (repassivation) behavior. The passive potential range, breakdown potential, and repassivation potential of a metal are surface-averaged parameters, which can be extracted and used for comparisons between specimens. However, the spatial distribution of breakdown sites makes it difficult to gain insight into structural breakdown mechanisms using only macroscale electrochemical methods.

Passive films are thought to be thermodynamically stable under in-service conditions or dissolve at such slow rates that the oxide is an effective barrier between a corrosive environment and the underlying metal substrate. Although passivation is widely accepted as the best method for corrosion protection and durability of metallic materials, compromise to a passive film through local degradation or physical damage can initiate localized corrosion.[1,40] The ability to repassivate requires that the metal contained in the passive film is readily available in the adjacent metal matrix for oxidation to reform the protective layer. Repassivation in many systems is poisoned in the presence of halides (Cl^-, Br^-, and F^-), which can promote the formation and growth of a pit and limit the material's self-protection from corrosion.[41,42] Pit propagation involves a high rate of anodic dissolution within a specific region whereas the rest of the surface is protected, which is difficult to detect, track, and measure using traditional surface-averaged electrochemical methods. The initiation of localized attacks has been attributed to differences in local passive film properties along a metal's microstructure, where local defects and/or differences in passive film characteristics (crystallinity and thickness) are vulnerable sites for passive film breakdown.[43] Localized corrosion can result in complete penetration of the metallic material and jeopardize the materials' mechanical integrity; therefore, it is important to explore and fully understand local passivity characteristics and passive metal's breakdown behavior.

2 | SCANNING ELECTROCHEMICAL PROBE MICROSCOPY METHODS

In situ scanning probe techniques, where a small probe is scanned across an interrogated surface, have greatly improved the understanding of passive film's nano and atomic structure, evolution, and breakdown under in-service conditions. For instance, electrochemical scanning tunneling microscopy (EC-STM) has enabled the direct observation of metal oxide formation and evolution at the atomic level.[8,10,32] However, due to EC-STM's high resolution, only microscopic and nanoscopic areas can be imaged, which decreases the probability of capturing a stochastic breakdown event. Furthermore, insulating passive films cannot be characterized using EC-STM due to the technique's operation principle based on quantum tunneling. Electrochemical atomic force microscopy (EC-AFM) allows for substrates covered with an insulating film to be imaged with high resolution, where topographical changes as a function of potential/current can be realized in situ.[44] Yet, like EC-STM, EC-AFM also images nanoscopic areas. Furthermore, both of these SPM methods are, except under special conditions, unable to collect local electrochemical information such as currents and ion flux.[45,46] Last, for both methods, the structure of an evolving corroding surface in solution may be too dynamic to be imaged with high confidence.

Alternatively, scanning electrochemical probe microscopy (SEPM) methods have been vital in understanding corrosion mechanisms and behavior,[47] including scanning vibrating electrode technique (SVET),[48] local electrochemical impedance spectroscopy (LEIS),[49,50] scanning Kelvin probe (SKP) and Kelvin probe force microscopy (KPFM),[51] scanning electrochemical microscopy (SECM),[52] and droplet cell techniques (scanning electrochemical cell microscopy (SECCM) and electrochemical droplet cell (EDC)).[53,54]

Of these methods, SECM, droplet cell techniques, and LEIS have been particularly useful for characterizing passive films on metals. This paper reviews previous studies that have utilized these SEPM techniques to characterize local passive behavior such as conductivity, film thickness, passive film discontinuation/defects, breakdown behavior, and repassivation capability for corroding metals. These characteristics can then be correlated to the underlying metal's microstructural features, including grain orientation, grain boundaries, inclusions, and chemical composition distribution using complementary microscopy and spectroscopy methods. First, the working principles and application to passive films of each SEPM reviewed are outlined. Next, SEPM studies on passive metal systems are presented by metal, including each metal's alloys. Finally, the outlook of SEPM to study passivity is discussed, including the local extraction of quantitative passive film parameters, the use of local alternating current (AC) methods and scanning ion conductance microscopy (SICM), and the optimistic future of SEPM techniques on advanced material/film systems.

Review
doi.org/10.1002/elsa.202300014
Chemistry Europe
European Chemical Societies Publishing

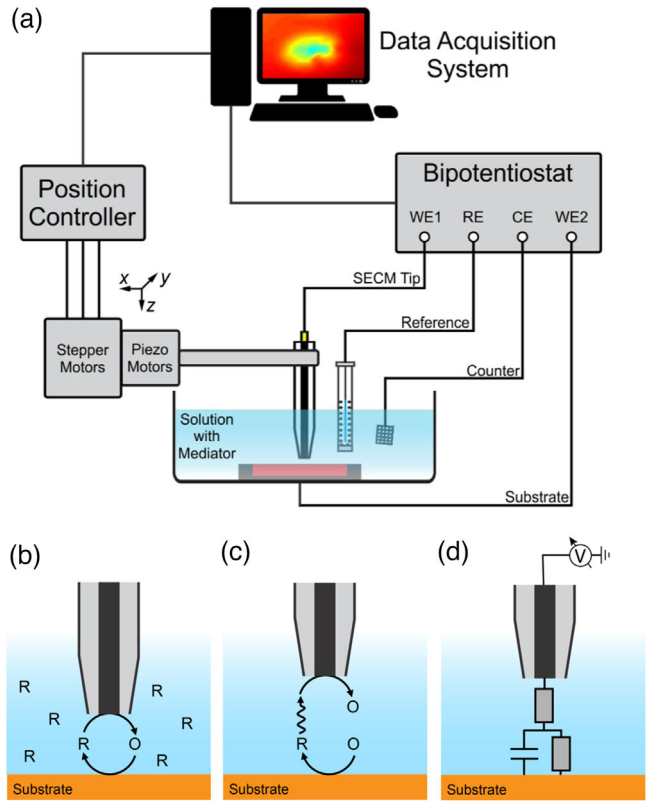

FIGURE 2 Schematic representation of (a) a scanning electrochemical microscopy (SECM) setupand an ultra-microelectrode (UME) probing a substrate in (b) feedback mode, (c) substrate generation tip collection mode as an example of a generation/collection (G/C) mode, and (d) bias-modulated mode where an alternating bias perturbation is applied the UME, commonly referred to as alternating-current scanning electrochemical microscopy (AC-SECM). Panel (a) is reprinted with permission from Polcari et al.[62] Copyright (2015) American Chemical Society.

2.1 | Scanning electrochemical microscopy

SECM has been applied in over 200 studies to investigate corrosion,[52] making this technique the most popular SEPM method utilized in corrosion science. Recent SECM-corrosion reviews are available that focus on the characterization of precursor regions for localized corrosion,[55] organic coatings,[56] and the use of ion-selective microelectrodes in corrosion studies.[57] A comprehensive review of SECM modes, experimental considerations, and advancements can be read elsewhere,[58] but the basic working principles and modes will be briefly described herein.

The scanning electrochemical microscope (Figure 2a) involves the movement of an amperometric ultra-microelectrode, or UME (<25 μm diameter disk), by a three-axis positioning system near the sample's surface (substrate) while immersed in an electrolyte containing at least one redox-active species, known as a redox mediator. A bipotentiostat is used to control and measure current/voltage at the working electrode UME (WE1) and possibly the substrate if the polarization of the sample during the SECM measurement is desired (WE2). The electrochemical setup is completed with a reference (RE) and counter electrode (CE) also immersed in the electrolyte that fills the electrochemical cell. Depending on the system being investigated (i.e., substrate conductivity, redox mediators present), different modes of SECM can be used. Modes that have been commonly utilized to study passive films on corroding metals include feedback mode,[59] generation/collection modes,[60] and AC modes,[61] which are described in the following sections.

2.1.1 | Feedback mode

The feedback mode of SECM is popular because of the simplicity of the experimental setup, where a redox mediator with fast kinetics at the UME is used to probe the substrate's kinetic activity (Figure 2b).[62] When the tip-to-substrate distance is greater than 10 times the radius of the electroactive UME area, a bulk steady-state current is measured from the hemispherical diffusion of the redox mediator toward the electrode surface where it can be oxidized or reduced.

$$R \rightarrow O + ne^{-} \quad (1)$$

where R is the reduced form and O is the oxidized form of the mediator. Typically, the UME potential is chosen well beyond the standard potential of the mediator to ensure that a Faradaic diffusion-limited current is measured.

When the microelectrode approaches the substrate, the diffusion field is perturbed by it, where the nature of the perturbation is dependent on the conductivity and electrochemical activity of the substrate toward the redox mediator. If the surface is electrically insulating, the mass transport of the redox mediator to UME tip is hindered and the current decreases as the probe moves closer to the substrate, termed negative feedback. If the surface is conductive, the redox mediator can be regenerated, and the current increases with decreasing tip-to-substrate distance. This type of behavior is termed positive feedback when the electrochemical reaction at the substrate and UME is diffusion limited (the kinetics are fast compared with the diffusion rate). It is also possible to measure the intermediate kinetic behavior, where kinetic and mass transport both contribute to the measured current.

It is common to perform an approach of the UME toward the substrate at a location of interest while measuring current to determine the electrochemical activity. These experiments are called approach curves, and in the case of intermediate kinetics, the heterogeneous reaction rate

constant of the redox mediator at the substrate can be obtained by fitting the data to analytical approximations or simulations.[63] Aside from approach curves, scanning the UME across the substrate in the *x*–*y* plane to build up a location/current map is used to visualize electrochemical heterogeneity. Careful analysis is needed to quantify kinetic rate constants from feedback mode images.[64–66]

2.1.2 | Generation/collection modes

In generation/collection (G/C) mode, an electroactive active species is generated either at the substrate and collected at a biased UME (substrate generation/tip collection (SG/TC)), or the UME and collected by the substrate (tip generation/substrate collection (TG/SC)), as shown in Figure 2c.[67] G/C mode is commonly used in corrosion studies to locally measure dissolved (corroded) metal ions along a corroding surface.[68–70] However, the collection efficiency may be low due to interference between the substrate and the tip reactions and fast diffusing species. G/C mode portrays lower spatial resolution compared to the feedback mode due to the interaction of the two diffusion fields of the UME and substrate.

2.1.3 | AC mode

Alternating-current scanning electrochemical microscopy (AC-SECM) mode involves applying a sine-wave perturbation to the UME to locally visualize impedance parameters, namely the local distribution of the electric double layer capacitance and charge transfer resistance, across a substrate (Figure 2d).[71] The advantage of AC-SECM over the bi- or tri-electrode LEIS is the increase in spatial resolution.[72–74] In the high-frequency domain, the UME can be positioned close to the substrate by measuring the resistance of the electrolyte.[75,76] The mapping of pitting corrosion can be realized at high frequencies, which also allows for rapid mapping of the sample.[77] In lower frequency domains, the impedance of the UME is sensitive to the local surface reactivity. Unlike other SECM modes, AC-SECM does not require the substrate to be biased or a redox mediator to be present, therefore enabling the investigation of corrosion processes locally under real-world conditions.[71]

2.2 | Electrochemical droplet cell and SECCM

Electrochemical droplet cell (EDC) methods enable direct electrochemical measurements to be carried out within a confined region along a substrate.[78,79] A microsized or nanosized glass pipette is filled with electrolyte and the meniscus formed at the opening of the pipette becomes the microsized or nanosized electrochemical cell. By adding a microquasi RE/CE wire into the back of the pipette, the miniaturized electrochemical cell can be approached to the working electrode, that is, the surface of interest. Once the micro/nanocell has been positioned to make electrical contact with the substrate, virtually any AC or direct current (DC) electrochemical measurement can be directly performed.[80–82] The dimensions of the pipette tip and wettability of the surface govern the technique's spatial resolution,[83,84] enabling quantitative electrochemical reactivity on the microscale and nanoscale to be obtained and used in convergence with other classical materials and electrochemical characterization methods. After analyzing a particular area, the droplet can either be scanned to another region of interest prior to initiating another local measurement (scanning mode), or, the probe can be retracted from the substrate (i.e., disconnected) and moved toward the next area before reapproaching the substrate (hopping mode). To avoid transferring corrosion products to another area, the hopping mode is most commonly used in corrosion studies.

The original EDC method by Suter and Böhni in 1997 was used to distinguish between active and inactive MnS inclusions present in austenitic stainless steel.[53] The experimental setup consisted of replacing a microscope lens with a micropipette and controlling the *x*,*y*,*z*-position of the sample using the microscope stage (Figure 3a). The size of the pipette implemented was typically on the order of 10–1000 µm and controlled the spatial resolution of the technique. A silicon gasket was used to make physical contact with the substrate to inhibit spreading/leaking of large droplets (Figure 3b). Since then, the evolution of EDC methods has gone from a manually positioned micropipette technique[78,79,85] to a rapid scanning electrochemical cell methodology.[86–88]

The use of SECCM (also known as the scanning micropipette contact method, or SMCM) in corrosion science has just begun to accelerate and is an exciting area in current research endeavors. The SECM positioning system and low current potentiostat have enabled the use of nanosized pipettes to rapidly screen an electrode's surface to obtain thousands of measurements on a single sample (Figure 3c). The use of machine learning and artificial intelligence can offer an unprecedented ability to process and extract meaningful information from these complicated and large datasets compared with the current capabilities.[89] Such efforts are likely to play a pivotal role in the future development of high-throughput SEPM studies of corroding systems. Electrolyte leakage is no longer an issue at these dimensions, although dynamic

Review
doi.org/10.1002/elsa.202300014
Chemistry Europe
European Chemical Societies Publishing

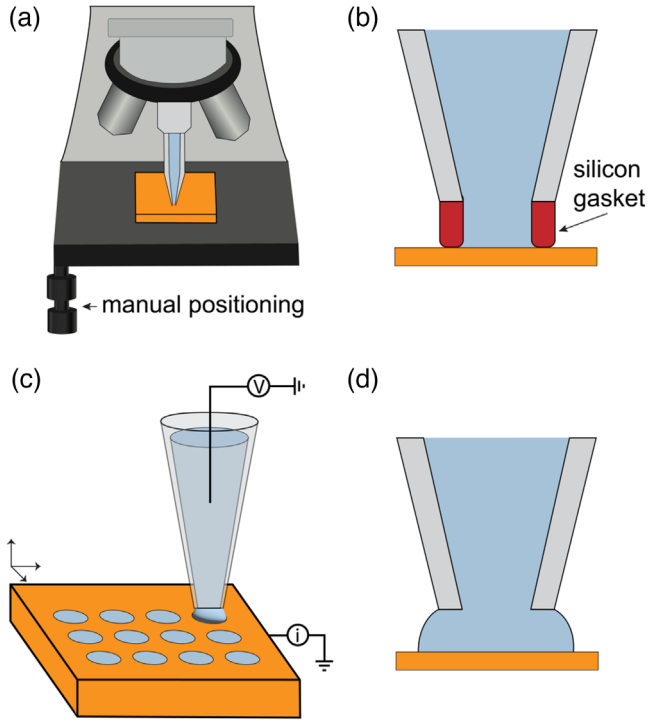

FIGURE 3 Schematic representations of electrochemical droplet cell methods. (a) The original electrochemical droplet cell (EDC) design that involves replacing a microscope lens with a micropipette and manually positioning the droplet onto the substrate using the microscope stage positioning system. (b) A close-up of a silicon gasket in EDC to isolate the working electrode surface area and avoid leakage. (c) The use of a single-channel micro/nanopipette in scanning electrochemical cell microscopy to enable systematic positioning/landing of thousands of droplet measurements on a single sample. (d) A close-up of the freely hanging droplet interacting with the substrate.

droplet spreading may be a concern when normalizing the measured current by surface area (Figure 3d).[84] Single or dual-channel pipettes can be used, although single channels have been mainly used for corrosion studies. As with SECM and other SEPM methods, complementary correlative microscopy and spectroscopy methods provide invaluable information about local surface chemistry that can be directly correlated with the local electrochemical response of passive films.

In addition to direct and local electrochemical imaging, there are several advantages of EDC methods in comparison with other SEPM techniques. The sample is not required to be fully immersed during imaging, where the contact region can be analyzed while the rest of the sample is left pristine (no aging effects). Measurements can be done without the need for a redox mediator. Last, the fabrication of micropipette and nanopipette tips with well-defined geometry is simple in comparison with the multistep assembly of a microelectrode used in SECM.[90]

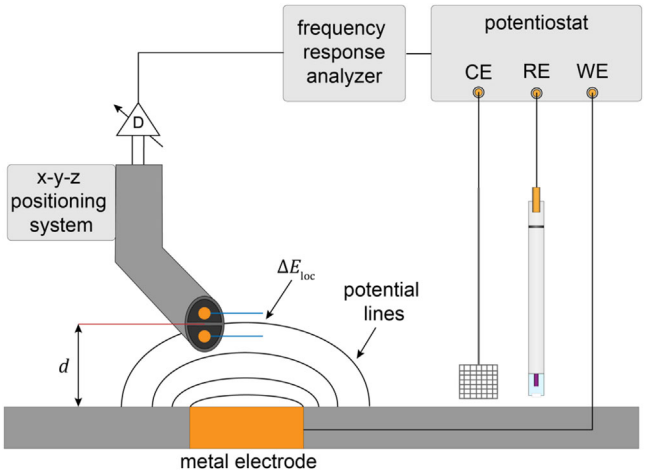

FIGURE 4 Schematic representation of the experimental setup for localized electrochemical impedance spectroscopy, where a dual-probe is positioned close to the substrate's surface to measure local oscillating potential gradients.

2.3 | Localized electrochemical impedance spectroscopy

LEIS is a nondestructive, AC method that enables localized impedance measurements of a conductive/semiconductive sample, thereby providing information on complex electrochemical processes.[91] The motivation to develop LEIS was the difficulty in interpreting conventional, surface-averaged EIS data when analyzing a locally corroding metal. The technique is based on the premise that in a macroscale three-electrode EIS measurement, the AC solution current densities close to the working electrode are proportional to its local impedance properties.[91] In a LEIS measurement, a potential perturbation is applied to the substrate while a dual-probe made of conductive material is positioned close to the substrate's surface (Figure 4). The AC solution current density, j_{loc}, normal to the electrode is calculated by measuring the AC potential drop, ΔE_{loc}, between planes parallel to the polarized substrate using the dual-probe:

$$j(\omega)_{loc} = \frac{\Delta E_{loc}\kappa}{d} \quad (2)$$

where κ is the solution conductivity, and d is the distance between the two probes. The local impedance, z_{loc}, can be derived from Eq3:

$$z(\omega)_{loc} = \frac{\Delta E(\omega)_{applied}}{j(\omega)_{loc}} \quad (3)$$

where $\Delta E_{applied}$ is the applied potential perturbation between the substrate and the reference electrode. LEIS

can be operated in two modes: single-frequency mapping or complete frequency sweeps at specific regions above the substrate to identify local changes in double layer capacitance, charge transfer, and ionic resistance. Like SECCM, LEIS has the advantage that a redox mediator is not required to locally measure these parameters.

3 | SEPM PASSIVITY STUDIES ON METALS

The following sections have been organized by passivating metals to discuss the use of SEPM methods to investigate local passive properties, behavior, and breakdown. We report the most insulating passive metal first, Al, and present other passivating metals and their alloys in order of decreasing band gap energy. The limitations of the SEPM techniques currently used for studying passive films will be discussed, followed by suggestions for future studies to quantitatively investigate film properties. The current literature will be summarized and the positive outlook on using SEPM to study passive films in corrosion science will be concluded.

3.1 | Aluminum

Aluminum (Al) is a common metal used as an alloy in the aerospace industry due to its high strength-to-weight ratio.[92] Al is also regularly used in metal components for energy storage devices, acting as current collectors[93] and/or casing materials for pouch batteries.[94] In air, Al spontaneously forms a 2–4 nm thick Al_2O_3 film that inhibits degradation of the underlying metal for a wide range of pH values.[95,96] Pure Al is known to be relatively corrosion resistant, where the natural passive film is electronically insulating with a band gap energy of 8.3 eV.[97]

However, the Al passive film contains electronic and/or microstructural defects, which are hypothesized to be related to film breakdown and subsequent pitting corrosion.[98] The observation of the Al passive film's behavior in a corrosive environment (i.e., chemical composition, adsorption/absorption of species, and hydration) in situ has been investigated using SEPM to probe the mechanism of localized corrosion of Al and Al alloys and relate it to such defects.

3.1.1 | SECM feedback mode to probe Al_2O_3 conductivity

In situ measurements of the local electrochemical behavior of naturally passivated Al were performed using SECM in feedback mode in a nonaqueous solution.[96] Al substrates of varying purity were polarized to a cathodic potential (−1.7 V vs. Ag/Ag^+) while SECM current mapping was performed. Regardless of purity, local electron-transfer sites with 1–10 μm effective radii were observed. The detected sites were speculated to be structural or electronic defects in the oxide film that hold unusually large electronic conductivity.[96] It was also mentioned that the defect sites could correspond to inclusions in the microstructure for the low-purity Al substrate. A follow-up SECM study on Al passive films was performed using two different redox mediators.[99] The measured electrochemical activity was independent of the redox mediator used, which may indicate that the electrical conduction at the defect sites (2–50 μm effective radii) was dependent on the electric field across the passive film and the interfacial potential applied. This was later confirmed by Jensen et al.[100] using a different set of redox mediators under aqueous conditions. The local electrical conduction of the substrate was determined to be sensitive to surface preparation, where the density of defects measured using SECM varied by 2–3 orders of magnitude depending on the preparation method used.[99] This finding is important to note, as metals can be pretreated using a variety of methods including mechanical polishing, deoxidation (cathodic cleaning/polarization), and/or chemical/electrochemical anodization. For instance, AC-SECM has been used to measure the local impedance response over an Al surface that had been anodized for incremental amounts of time (Figures 5a–d).[61] The local film capacitance and film thickness maps showed that the passive film had grown from ∼4 nm to ∼25 nm after just 3 min of anodization.[61] Although a 25 μm Pt UME was used, the generated maps were on the order of mm, where further investigation at small regions would be necessary to resolve film thickness on individual grains. A similar spatial resolution was reported for the original study on the localized impedance of Al using LEIS.[91] Each pretreatment method/step can influence the formation of the natural surface oxide, and therefore the number and distribution of defect sites. A systematic SECM study of how pretreatment influences passive film defects would be beneficial.

3.1.2 | Generation mode: Inducing pitting corrosion on Al

The G/C mode of SECM was used to generate a local concentration of chloride ions to initiate a single pit on pure Al.[60] The measured current at the Al substrate continued to increase even after chloride generation halted. The hypothesis was that the formation of the pit was likely linked to the aggressive ion generation at the SECM tip, and once initiated, the current to sustain pitting was

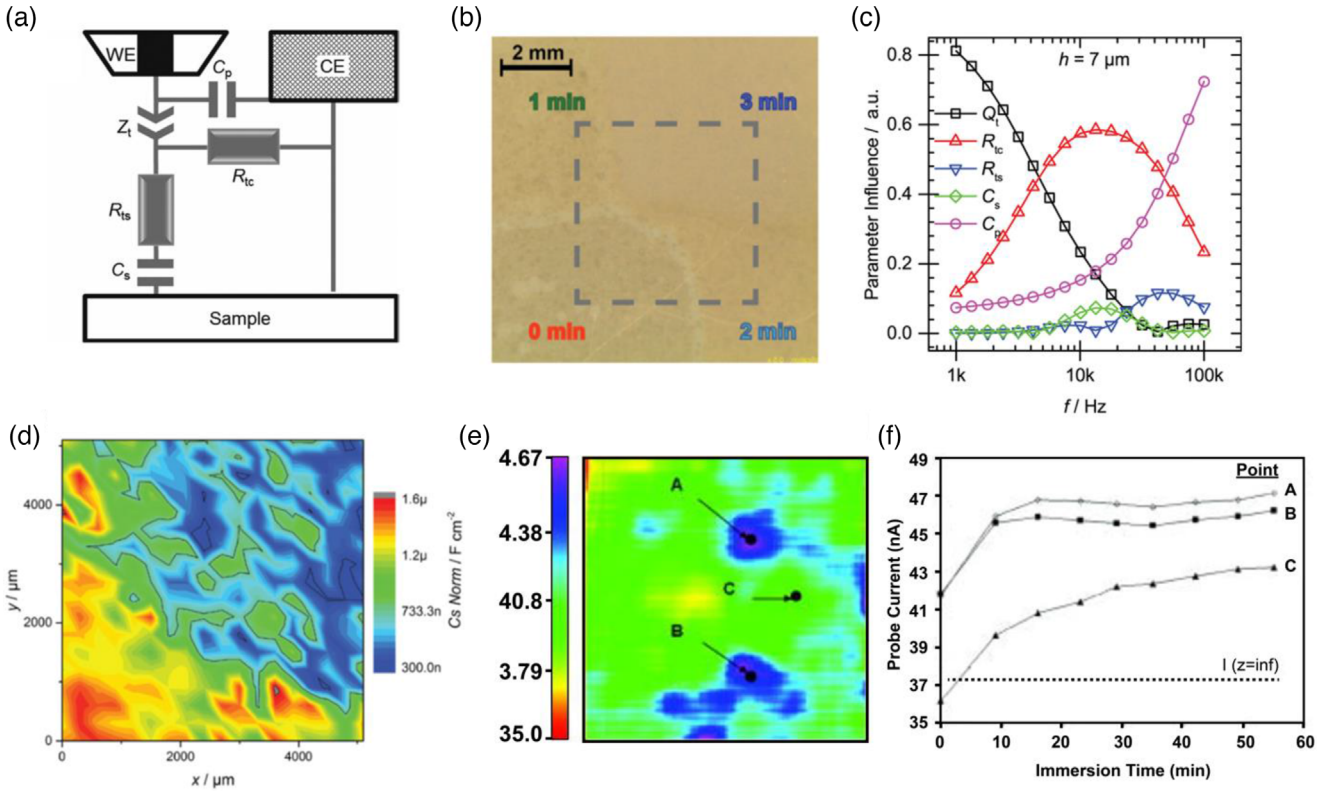

FIGURE 5 (a) The equivalent electrical circuit (ECC) used to fit the scanning electrochemical impedance microscopy data for charge transfer inhibiting systems. (b) An image showing the four zones anodized Al in H_2SO_4 for specified times, with the AC-SECM (alternating-current scanning electrochemical microscopy) scan area indicated by a dashed line. (c) Influence diagrams for the five circuit components used in the ECC used to fit local EIS spectra 7 µm above the anodized Al in 1 mM $KClO_4$. (d) The normalized capacitance maps from local EIS spectra 7 µm above the substrate. (e) an SECM image of the AA 2024-T3 Al alloys held at a potential of −0.8 V versus Ag/AgCl in 0.01 M hydroquinone (HQ), 1.0 M Na_2SO_4, and 0.005 M H_2SO_4 after immersion of 9 min. (f) Probe current as a function of immersion time for points A, B, and C as indicated in the SECM image in (e). (a–d) Reprinted with permission from Estrada-Vargas et al.[61] Copyright (2016) American Chemical Society. (e and f) Mark B. Jensen et al.[100] https://doi.org/10.1149/1.2916734. © The Electrochemical Society. Reproduced with permission from IOP Publishing Ltd. All rights reserved.

due to the low pH conditions (pH~2.4).[60] Further studies involving SECM-initiated pitting as a function of pH, substrate potential, and chloride ion concentration would be valuable to better understand each parameter's influence on passive film breakdown and localized corrosion of Al. The rate of pit growth and corrosion product could also shed light on the breakdown process. The combination of G/C mode and feedback mode would enable the preselection of pitting sites, for instance, at "defects" (i.e., inclusions and/or grain orientations) in the passive film and at protected (insulated) regions, to evaluate the breakdown rate as a function of surface heterogeneity.

3.1.3 | Al alloys

The use of alloying elements in Al increases the material's strength through the formation of secondary phases. The resulting microstructure includes alloying element-rich inclusions that often portray different electrochemical potentials to the Al matrix and cause microgalvanic coupling that initiates localized corrosion. The two most widely used Al alloys for the 2xxx series (Cu is the main alloying element) and the 7xxx series (with Zn, Mg, and Cu as alloying elements), which give excellent mechanical properties, yet are susceptible to corrosion.[101,102]

3.1.4 | SECM feedback mode to probe alloy passive film conductivity

A study compared the electrochemical activity of pure Al and the Al alloy, AA 2024-T3, using SECM in feedback mode.[100] Both the oxidation and reduction capabilities of the materials were investigated using two different redox mediator systems that either were reduced or oxidized at the substrate. By correlating the Al alloy's microstructure via scanning electron microscopy and energy dispersive

X-ray spectroscopy (SEM/EDX) back to local reactivity observed in SECM current maps, it was found that Cu-containing inclusions showed the highest electronic transfer activity for both mediators and over a 60 min immersion time (Figures 5e and f). The independence of reactivity from redox mediator types was confirmed for pure Al, where both oxidation and reduction electron transfer occurred at the same defect sites.[100] However, the probe currents measured over pure Al were lower compared with the values extracted over the Al alloy for acidic and neutral conditions, indicating lower electron transfer rates on pure Al and therefore a more protective oxide film. Higher reactivity over Cu-rich inclusions in an Al alloy was confirmed by Seegmiller and Buttry.[103] In general, findings from SECM studies over Al alloys indicate a difference in the nature of the passive film (or lack thereof) over the intermetallic and/or secondary phase inclusions.[104,105] This corroborates with atomic force microscopy/scanning elcetrochemical microscopy (AFM/SECM) studies performed on some Al alloys, where localized anodic dissolution has been measured via electrochemical activity and changes in topography in the boundary region adjacent to large intermetallic particles.[106–109] The particles show cathodic activity and result in a microgalvanic effect on the surrounding metal matrix where local dissolution can occur at this vulnerable point.

3.1.5 | Effect of grain orientation on Al passivity

Using the EDC, Krawiec and Szklarz showed that plastic deformation led to an increase in pitting susceptibility due to a higher density of dislocations in the passive film.[110,111] This was found to be independent of grain orientation. A recent study that utilized SECCM and electron backscatter diffraction (EBSD) on a polycrystalline Al alloy provided information about local breakdown events at defective film regions (Figure 6a). Over 2511 micro-potentiodynamic polarization (micro-PDP) measurements were performed at discrete locations along the material's surface using a solution of 3.5 wt% NaCl (Figure 6b).[112] By correlating the current response to grain orientation (and neglecting responses at intermetallics and grain boundaries), it was found that the <101> orientation portrayed the largest cathodic and anodic currents (Figures 6c and d). This finding was consistent with the predicted surface energy of the different grains,[113,114] where the loosely packed <101> plane has fewer atoms (lower atomic planar density) and higher surface energy. Therefore, more sites for cathodic reactions are available, as well as the facilitation of Al atom ejection from the bulk metal (corrosion), which indicated a higher corrosion rate over this grain orientation. The SECM-detected defects in the passive film formed over pure Al[96] may be the result of the difference in passive film conductivity via tunneling over different grain orientations, especially since the SECM studies involved polarizing the Al substrate.

The susceptibility of pitting corrosion was determined by a lower breakdown potential, which would suggest a more defective passive film structure that would enable ionic migration and lead to passive film breakdown (Figure 6e). Although <101> grains showed higher electrochemical activity, there was no correlation between the number of pitting locations shown as a function of pitting potential for each grain orientation (Figures 6f and g).[112] This suggested that the nature of the passive film may play a more dominating role in determining the localized corrosion initiation in comparison with the grain orientation. Further, the increase in conductivity of the passive film at local regions may not correlate to defect sites that have a higher probability of local passive film breakdown, as previously hypothesized in SECM studies.

3.1.6 | Time dependence of Al repassivation

The ability to repassivate after the selective dissolution of intermetallics in Al alloys has been suggested by Jensen et al.[100] Upon changing the pH and substrate potential during imaging, a region that originally showed activity became invisible to SECM. This was proposed to be due to repassivation of that region after inclusions with a certain elemental composition were dissolved from the alloy's surface. The regeneration of the redox mediator was also measured during an immersion study in an acidic solution (pH ~2–3). It was found that the electronic behavior of the substrate changed from insulating to conducting with increasing immersion time (~1 h), indicating the dissolution of the Al matrix and minimal protection from the passive film. In neutral conditions, the insulating nature of the passive film remained constant, and therefore stable, with increasing immersion time.[100] A recent study showed that SECM could be used to monitor in-situ repassivity after physically damaging the natural passive film on an Al alloy.[104] Although not the aim of the investigation, it was observed that the magnitude of current measured using SECM in feedback mode over a scratched area decreased over 24 h during immersion.

3.1.7 | Future work using SEPM on Al

Although inclusions in low-purity Al and Al alloys have been determined to be electroactive defect regions in the

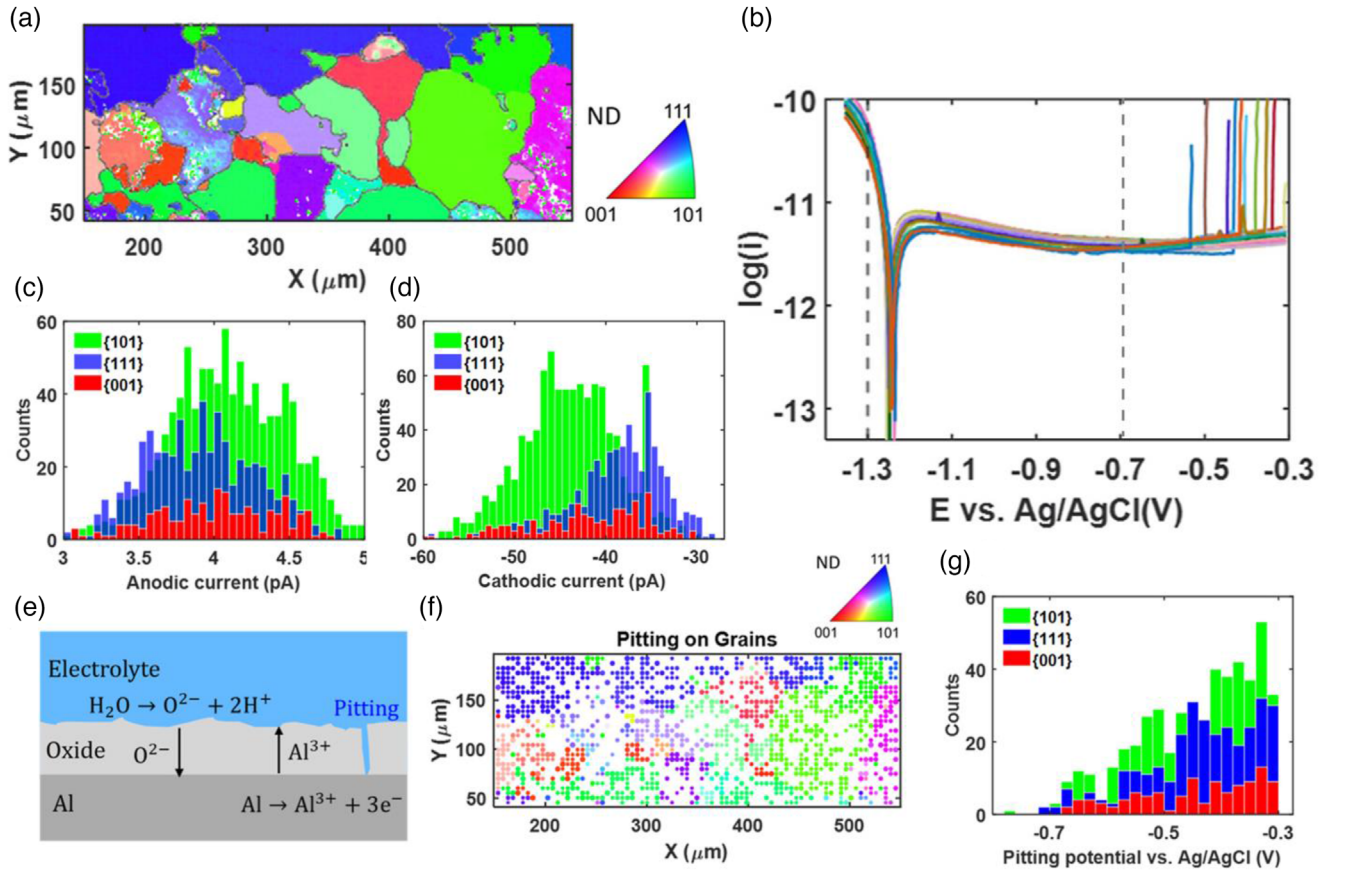

FIGURE 6 (a) Electron backscatter diffraction color map presenting the grain orientations of AA7075-T73 Al alloy with respect to the sample normal direction (ND). (b) 26 randomly chosen micro-potentiodynamic polarization curves measured using scanning electrochemical cell microscopy. (c) Presentation of the statistical distribution of anodic currents (at 0.7 V vs. Ag/AgCl) measured on different crystal planes. (d) Presentation of the statistical distribution of cathodic currents (at −1.3 V vs. Ag/AgCl) measured on different crystal planes. (e) Schematic representation of the ionic migration and breakdown of the passive film to induce pitting. (f) Demonstrating the pitting occurrences on different grains. (g) Presentation of the statistical distribution of pitting events occurring at different potentials on different crystal planes. Adapted with permission from Li et al.[112] Copyright (2022) American Chemical Society.

passive film, the origin of defects (i.e., regions of higher conductivity) on high-purity Al samples was not hypothesized or investigated. Systematic studies on pure Al should be conducted to reveal the nature of the defects. In addition, the relationship between passive film growth (thickness and defects) and grain orientation remains unclear for Al. Future time-of-flight secondary ion mass spectrometry (TOF-SIMS) studies could also elucidate the relationship between pitting susceptibility and film thickness, similar to a recent SECCM study on Ni.[115]

3.2 | Zirconium

Zirconium (Zr) alloys are materials that are extensively used in aggressive industrial applications, particularly in nuclear and chemical industries, due to their excellent mechanical and corrosion properties.[116] With a low neutron absorption cross-section, Zr has many uses inside a reactor core to fabricate components such as fuel cladding and calandria vessels.[117]

The corrosion resistance of Zr is due to the formation of an insulating (bandgap of 5.7 eV) ZrO_2 passive film.[118] The passive film also provides an excellent barrier to hydrogen ingress that can cause brittle hydride phase formations that jeopardize the mechanical stability of the material under tension.[119] Zr and alloys portray a bi-phasic microstructure containing α and β-phases. In commercially pure Zr, Fe is commonly present and has been found to increase the local electrical conductivity of ZrO_2 surface films.[120] Alloying elements have also been added to Zr to influence the material's mechanical properties and corrosion resistance.[121] For instance, Zircaloy-2 alloy contains Cr, Fe, Ni, and Sn. It was shown that Sn is contained with the α-phase,[122,123] whereas Cr, Fe, and Ni segregate in the β-phase to form Zr $(Fe, Cr)_2$ and $Zr_2(Fe, Ni)$ intermetallics.[123,124] The intermetallic inclusions in both pure and Zr alloys have been proposed

Review
doi.org/10.1002/elsa.202300014
Chemistry Europe
European Chemical Societies Publishing

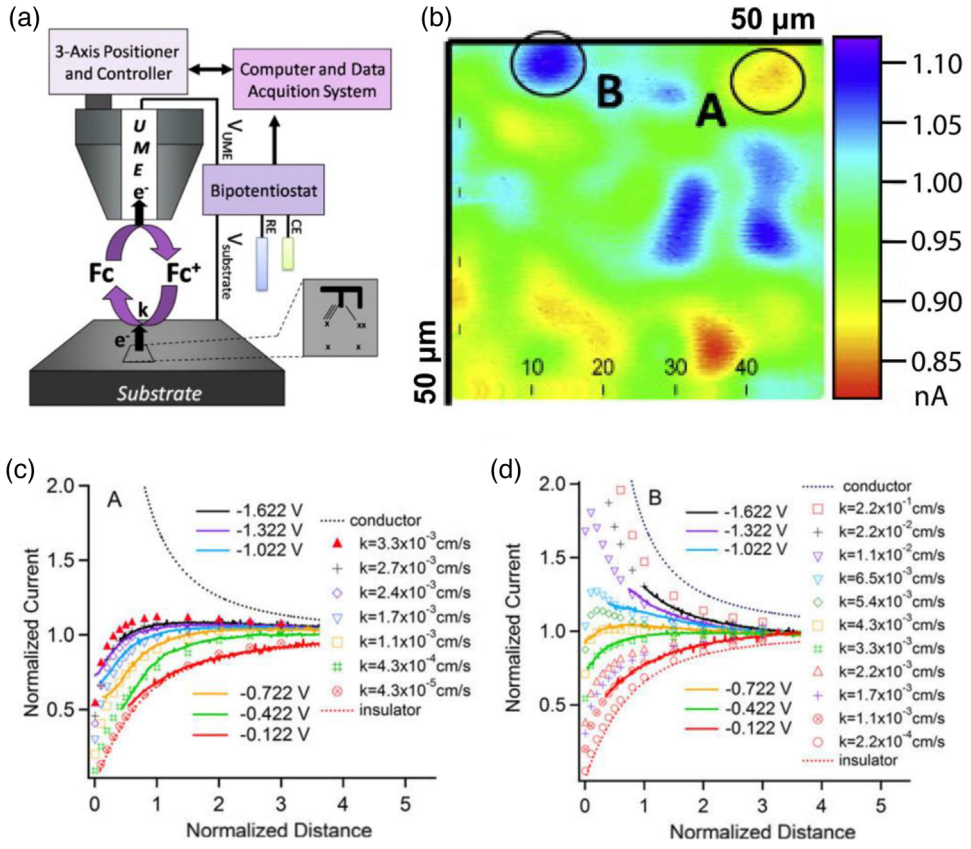

FIGURE 7 (a) Experimental setup for feedback mode study on Zr. (b) Scanning electrochemical microscopy image over Zr after 24 h recorded in 0.9 mM ferrocenemethanol and 0.1 M Na_2SO_4 solution (50 × 50 µm, 7 µm carbon microelectrode). The microelectrode and sample were polarized to 0.23 and −1.62 V versus saturated calomel electrode, respectively. (c) Approach curves over regions A and B (from (b)) at different substrate potentials with simulation curves for different kinetic constants at the surface. Reprinted from Nowierski et al.[126] Copyright (2009) with permission from Elsevier.

to be sites for hydrogen ingress into the metal and hence their reactivity should be quantified.

To investigate the local electrochemical activity of intermetallic impurities found in Zr, SECM in feedback mode has been employed (Figure 7a).[125] The generation of ferrocenemethanol (FcMeOH) occurred at a faster rate over Fe inclusions than the insulating passive film (Figure 7b). Cathodic polarization led to a small increase in feedback current, which was attributed to the thinning of the passive film (Figure 7c).[125] Upon cathodic polarization, partial positive feedback was measured over the Fe impurities (Figure 7d). The faster reduction of the redox mediator at these locations indicated that the passive film was either less coherent and/or more readily reduced.[125]

Another SECM study using FcMeOH in feedback mode was done to investigate the effect of alloying elements in Zircaloy-2 on local reactivity.[126] Like the study performed on pure Zr, it was found that Fe, Ni, and Cr-rich inclusions were reactive spots under cathodic polarization. These inclusions were located within the β-phase grain boundaries and suggested to act as "windows" for hydrogen absorption into the alloy.[126] The Sn containing α-phase grains remained passive even at very low applied cathodic potentials of −2.0 V versus saturated calomel electrode (SCE).

3.2.1 | Future work using SEPM on zirconium

As far as the authors are aware, these two studies are the only reports on using SEPM methods to study localized electrochemical properties of Zr. Although the studies do provide evidence of reactive inclusions that portray different reactivity than the passivated metal matrix, it remains unclear what the driving feedback mechanism is since only redox mediators that undergoes reduction at the substrate was implemented. If the inclusions were to be etched away during SECM feedback measurements, this would suggest that they were not covered in a protective passive film and were vulnerable to dissolution. Studies using SECM in G/C mode and/or SECCM could elucidate whether the inclusions (electro)chemically dissolve.

3.3 | Nickel

Nickel (Ni) and Ni alloys are commonly used for alkaline oxygen evolution reactions,[127,128] sea water electrolysis,[129,130] Ni-based batteries,[131,132] and in other aggressive corrosive environments.[133,134] Ni spontaneously forms a protective passive film when exposed to aerated environments that is composed of nickel (II) oxide (NiO).[15] The passive film formed anodically portrays a p-type electronic character, which corresponds to metal vacancies. At large anodic potentials (>1 V vs. SCE), the film shows some n-type character that has been attributed to the presence of electrons from the oxygen evolution reaction and/or ejection of Ni^{3+} from the outer layer interface.[15] The transpassive state of Ni has been hypothesized to be comprised of a thick, porous oxide film that would be vulnerable to localized attack. Indeed, with a band gap energy of 3.5 eV, Ni and Ni alloys are susceptible to localized corrosion, especially crevice corrosion.[133]

3.3.1 | Passive film breakdown on Ni

The first SEPM study on Ni focused on the role of sulfide inclusions on localized corrosion parameters in chloride-containing solutions.[135] Ni200 (0.25% Cu, 0.4 % Fe, 0.15 % Si, 0.1 % Ti, <0.0018% S, Ni balanced) portrayed pitting corrosion surrounding sulfide-rich inclusions using macroscale PDP measurements. Direct local PDP measurements using a microdroplet cell showed that variation in pitting potential increased when using smaller microcell diameters, which was attributed to the randomness of the number of inclusions. SECM studies showed that dissolved sulfur-containing species deposited near the inclusion before and during pit growth. Although inclusion distribution may play a role in variability detected using SEPM, other microstructural properties have been found to play a more critical role in local passivity breakdown.

SECCM was utilized by Li et al.[115] to directly reveal the variability in the breakdown potentials of NiO film on polycrystalline Ni (Figure 8a). By correlating SECCM analyzed areas with EBSD, it was shown that the Ni grains in a crystal orientation close to <111> were more resistant to breakdown, where no pits formed during the voltammetric scan up to 2 V versus Ag/AgCl (Figures 8b–d). TOF-SIMS was used to correlate the heterogeneity of passive film stability with oxide thickness. Surprisingly, the stability of the passive film was higher for thinner NiO films, which was rationalized using classical nucleation theory (Figures 8e and f). This study also demonstrated the ability of SECCM to measure preferential passive film breakdown directly and locally at the grain boundaries of Ni to provide information about intergranular corrosion susceptibility. This work sheds light on a likely reason for the variability in local breakdown potentials determined in previous studies.[135]

3.3.2 | Ni alloys

Most of the Ni produced is used to fabricate alloyed materials, either Ni-rich alloys or as an alloying element.[133] A recent study focused on using SECM in feedback mode and EBSD to quantify the electrochemical reactivity of the passive film formed over different grain orientations for the Ni 600 alloy (Ni–16Cr–8Fe).[136] The results revealed passive film anisotropy, where the conductivity of the passive films increased over grains with a higher misorientation angle from the <111> plane. This finding is in agreement with previous AFM studies on Ni alloy 600 that found that the surface oxide morphology directly related to the orientation of the underlying crystal.[137] The lower conductivity measured using a redox mediator that undergoes oxidation at the substrate over the <111> orientation correlates well with the SECCM study performed on pure Ni, which demonstrated the highest resistivity to breakdown yet the thinnest oxide film coverage.[115] This may mean that the thinnest passive film is most resistive to pitting and highly insulating, which suggests that conductivity does not necessarily scale with film thickness.

The near-equiatomic Ni titanium (Ti) alloy called nitinol (TiNi) is a superelastic material that is commonly used in the medical industry due to its excellent corrosion resistance and biocompatibility.[138,139] The formation of a titanium oxide (TiO_2) passive film over the TiNi substrate is similar to the oxide film found on Ti alloys and is responsible for the material's corrosion resistivity in comparison with Ni.[140] However, the enrichment of Ni in the passive film makes nitinol susceptible to localized (pitting) corrosion.[141,142]

The visualization of inhomogeneities over a passivated nitinol surface was first achieved by Schulte et al.[143] using AC-SECM. Local changes in solution resistance were attributed to variations in electrochemical activity while anodically polarizing the material to 1.9 V versus Ag/AgCl in a chloride-rich environment. This approach enabled the evolution of corrosion pits to be monitored with high spatial resolution. The passive behavior of nitinol under electrochemical polarization was further investigated by others using a variety of SECM modes.[69,144,145] The separation of anodic and cathodic sites was detected after anodic polarization using SECM in feedback mode, where further potentiometric SECM studies revealed local acidification over anodic regions involving Ni dissolution, and alkalinization over cathodic regions.[69] The insulating behavior of the passive film on nitinol was determined in

Review
doi.org/10.1002/elsa.202300014
Chemistry Europe
European Chemical Societies Publishing

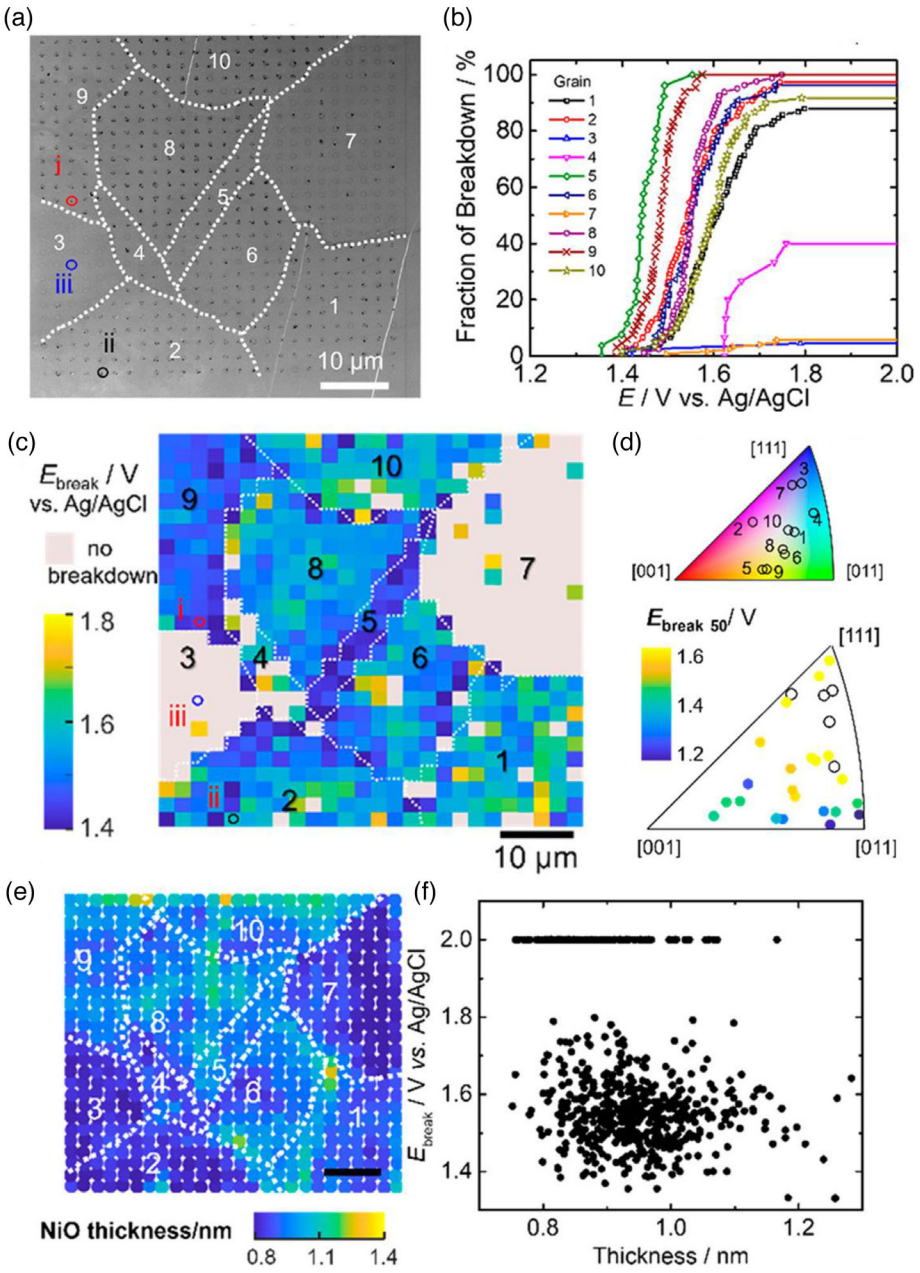

FIGURE 8 (a) A scanning electron microscopy image of the scanned area on Ni with scanning electrochemical cell microscopy (SECCM) showing the footprint and pits formed after localized voltammetry measurements. The grain boundaries are indicated by the dashed lines. (b) The distribution of cumulative probably of locations where pits have formed as a function of applied potential for different grain orientations. (c) An SECCM map of the breakdown potential on different grains imaged. The gray areas show scans up to 2 V versus Ag/AgCl that did not undergo pitting. (d) A stereographic triangle plot of the breakdown potential when 50% of the locations showed pitting on each grain. (e) Time-of-flight secondary ion mass spectroscopy map of NiO layer thickness. The scale bar is 10 μm. (f) Breakdown potential as a function of local NiO thickness. The data at 2 V represent measurements that did endure breakdown. Reprinted with permission from Li et al.[115] Copyright (2022) American Chemical Society.

another feedback SECM study by the smaller tip current measured when biased to low potentials. Yet, film breakdown was confirmed when polarized to higher anodic potentials by the large current detected at the microelectrode during SG/TC mode from Ni dissolution.[144] This study indicated that there is a time dependence on film conductivity with film growth that may play a role in the material's ability to undergo repassivation. A time-dependence study of passivation correlated to the material's microstructure (e.g., grain orientation, grain boundaries, inclusions) would provide insight into the local repassivation behavior.

Review
doi.org/10.1002/elsa.202300014
Chemistry Europe
European Chemical Societies Publishing

Stripping and AC modes of SECM were used to investigate the passivity of a nitinol and stainless steel laser weld interface.[146] The combination with other corrosion-resistant materials can be desirable to reduce costs, as nitinol is an expensive and difficult-to-machine material. A decrease in electrochemical activity and dissolved Ni concentration over the dissimilar welded surface was evidence of better passivation compared with SECM results over single stainless steel or nitinol, possibly due to a synergistic effect of Cr and Ti in the protective oxide. Further surface chemistry characterization of the bi-elemental passive film could provide insight into new passivating alloys for biomedical applications.

3.3.3 | Time dependence of Ni repassivation

SECM in feedback mode was used to study the passivating and repassivating behavior of nitinol when exposed to acidic media.[147] The loss of passivity was detected by the increase in electron transfer reaction rate at the alloy's surface after immediate exposure. The dissolution of the NiO in the passive film was confirmed by the increase in the Ni species in solution. The self-healing properties of the Ti-rich oxide film were observed using SECM approach curves, taking several minutes to repassivate. This study verified the need to understand nitinol's repassivation behavior due to concerns of usage in low pH physiological environments as Ni ions cause adverse health issues.[148–150] Local quantification of Ni release using the stripping mode of SECM in acidic media could be of interest to relate locally determined Ni concentrations to the material's microstructure to correlate metal dissolution with vulnerable areas of localized attack.

3.3.4 | Future work using SEPM on Ni

Most SEPM measurements on Ni do not spatially quantify the reactivity of the materials using approach curves. For instance, most studies use a single approach curve to represent the kinetics of the entire surface mapped. However, microstructural differences, including grain orientation, grain boundaries, and inclusions may portray different reactivity. The correlation between the breakdown location and the material's microstructure could provide better insight into localized corrosion initiation mechanisms. This was demonstrated by Li et al.'s work using SECCM to investigate polycrystalline Ni, where grain orientation was correlated to the passive film's thickness. Further investigations using correlative microscopy methods should be carried out to better understand the relationship between inclusion sites and local passive film breakdown.

3.4 | Titanium

Ti and Ti alloys are readily used as materials for biomedical devices,[151] catalysis,[152] and within the aerospace sector[153] due to their high corrosion resistance. Ti and Ti alloys spontaneously passivate when exposed to air. Conditions during passivation—including applied potential andsweep rate during anodization, surface preparation, and chemical environment —dictate the nature, composition, and thickness of the Ti passive film.[154–157] It has been shown that passive films on Ti consist of a layered structure of Ti oxides, where the oxygen content decreases from TiO_2 at the film/electrolyte interface to Ti_2O_3 and TiO near the film/metal interface.[158] TiO_2 is an n-type semiconductor, where oxygen vacancies[159,160] and Ti^{3+} interstitials[161] have been reported to be the main defects and electron donor species within the passive film.

Although the passive film formed on Ti is protective in many environmental conditions (e.g., breakdown potential >10 V versus SCE in chloride-containing solutions),[162,163] Ti and alloys are not immune to localized corrosion. Crevice and pitting corrosion occur in the presence of bromide and result in passivity breakdown and high dissolution rates.[162–164] Some studies rationalized this unusual behavior by suggesting that: the specific adsorption of Br^- at the oxide surface and the formation of soluble oxy-bromide Ti(V) salts cause local thinning,[164,165] the presence of impurity (Fe-rich) sites invoke the formation of TiBr and cause pit initiation after reaching a critical concentration,[166] or that the formation of surface Ti peroxo-species through electrochemical reactions between the passive film and the electrolyte change the ionic and electronic properties of the TiO_2 film.[163] SEPM studies have been carried out on Ti and Ti alloys to elucidate the passive film breakdown mechanism and to locally characterize the material's activity.

3.4.1 | Passive film breakdown on Ti

White and coworkers' study using SECM in feedback mode on Ti foils was the first corrosion-related SECM investigation reported to measure the local electrochemical activity of a corroding substrate.[167] They demonstrated that Br^- is electrochemically oxidized at localized, microscopic sites along the TiO_2 surface that show high electrochemical activity before pit nucleation. The rapid electron-transfer rate for Br^- oxidation at localized sites was attributed to either an increase in the electronic conductivity of the passive film or specific composition and/or structure of the oxide that enabled an interfacial catalytic effect.[167] Supporting research for the spatial variability in passive film conductivity has been documented using scanning

doi.org/10.1002/elsa.202300014

tunneling microscopy (STM)[168] and conductive AFM (C-AFM).[169]

Another SECM study estimated that the randomly positioned surface sites where the oxidation of Br^- occurred were 10–50 μm in diameter.[170] This work confirmed that the location of electroactive sites correlates to pitting along the Ti surface when the breakdown of the film was initiated by anodic polarization. A proposed mechanism for Br^- induced pitting corrosion was presented. First, the preferential oxidation at microscopic surface sites at potentials above the thermodynamic redox potential for the redox couple but below the potential of passivation film thickening. This is followed by a decrease in the electron-transfer rate due to the thickening of the oxide. Finally, the chemisorption of Br^- occurs at potentials corresponding to the onset of pitting at the microscopic sites. The authors concluded that pitting susceptibility was associated with oxide film defects observed using SECM, but the type or cause of the defects was not investigated using complementary microscopy techniques. Potential defects include inclusions, mechanically formed defects, and structural defects due to the underlying crystallographic orientation.

The nature of the defects has been explored further using SECM. The preferential oxygen evolution on a polycrystalline Ti electrode was detected over grains that wer covered with a thinner passive film,[171] although local film thicknesses were not reported. Later studies using C-AFM revealed a 200× increase in conductivity of oxide films on grain boundaries than films on grain faces.[169] This is a likely consequence of the structural mismatch of oxide films growing at different rates on neighboring grains to result in highly nonstoichiometric and defective films formed over grain boundaries. Spatial variations in oxide film conductivity on grain faces were also observed and predicted to be related to differences in film crystallinity.[169] It is unlikely that the locally active defect sites on Ti/TiO_2 detected using SECM can be solely attributed to a difference in film conductivity for oxides formed over grain boundaries, as the defects occupy a remarkably small percentage of the total exposed area (0.01–0.1%).[172] Regardless of the defect's nature, they either correspond to regions of a sufficiently thin oxide film that enables electron tunneling or regions where the local stoichiometry and/or impurity levels within the film differ and result in different oxide layer electronic conductivity.[172] Future correlative microscopy methods with SECCM on Ti should be performed to directly quantify film thickness on different grain orientations and correlate the number of breakdown sites statistically.

The potential dependence of the localized electrochemically active sites at passive Ti surfaces was measured using a variety of redox mediators that undergo electron transfer at potentials within or below the Ti oxide bandgap.[173] Mediators that undergo electron transfer at potentials within the oxide bandgap provided positive feedback during SECM measurements, showing that the microscopic (defect) sites had metal-like properties at potentials where the passive film should be insulating.[173] The oxidation (corrosion) of these metal-like sites could have been accelerated by the SECM measurement to enable the regeneration (reduction) of the redox mediators. This also demonstrated that the spatial electrochemical activity was not dependent on Br^- adsorption. For species that undergo electron transfer at potentials negative of the conduction band (and undergo oxidation at the substrate), the electrochemical response was uniform across the passive Ti surface and did not reveal the microscopic sites that were detected with mediators that undergo reduction at the substrate. This study confirmed that the electrochemical behavior of the Ti passive film was consistent with the model of an n-semiconductor containing defect sites with high electronic conductivity.

The use of redox mediators that undergo reduction at the substrate and reduce at potentials below the TiO_2 conduction band have been frequently used to explore the passive film behavior of pure Ti. FcMeOH was employed to measure the SECM feedback behavior on Ti passive films during substrate polarization (Figure 9).[144,174] Upon anodic polarization toward positive potentials (0.35 V versus Ag/AgCl), the passive film feedback response portrayed insulating behavior (Figures 9a and b).[144] This was attributed to the probable increase in film thickness, although film growth has been previously shown to occur only at larger anodic potentials.[170] Cathodically polarizing Ti had the opposite effect, where the kinetic rate constant of FcMeOH increased two orders of magnitude and demonstrated a more conductive film (Figure 9c).[174] The approach curve results were in good agreement with SECM current maps that showed the uniform increase in conductivity of the cathodically polarized Ti substrate (Figure 9d). It is interesting to note that although both studies were performed in similar solutions (chloride containing and neutral pH), the approach curves obtained at open circuit potential (OCP) differed greatly from negative (insulating) to positive (conducting) behavior. This is likely due to the difference in film thickness, where the Ti electrode that portrayed positive feedback was naturally passivated, whereas the negative feedback response was collected over an electrode that was first polarized at 2 V versus Ag/AgCl for 60 s to form a thick, anodically grown oxide film. This differing behavior emphasizes the need to investigate the effect of possible film growth during immersion in the SECM test solution to decouple the effect of conductivity due to a difference in passive film thickness or from defects in the film. Further, surface pretreatments can greatly impact the electronic structure of the passive

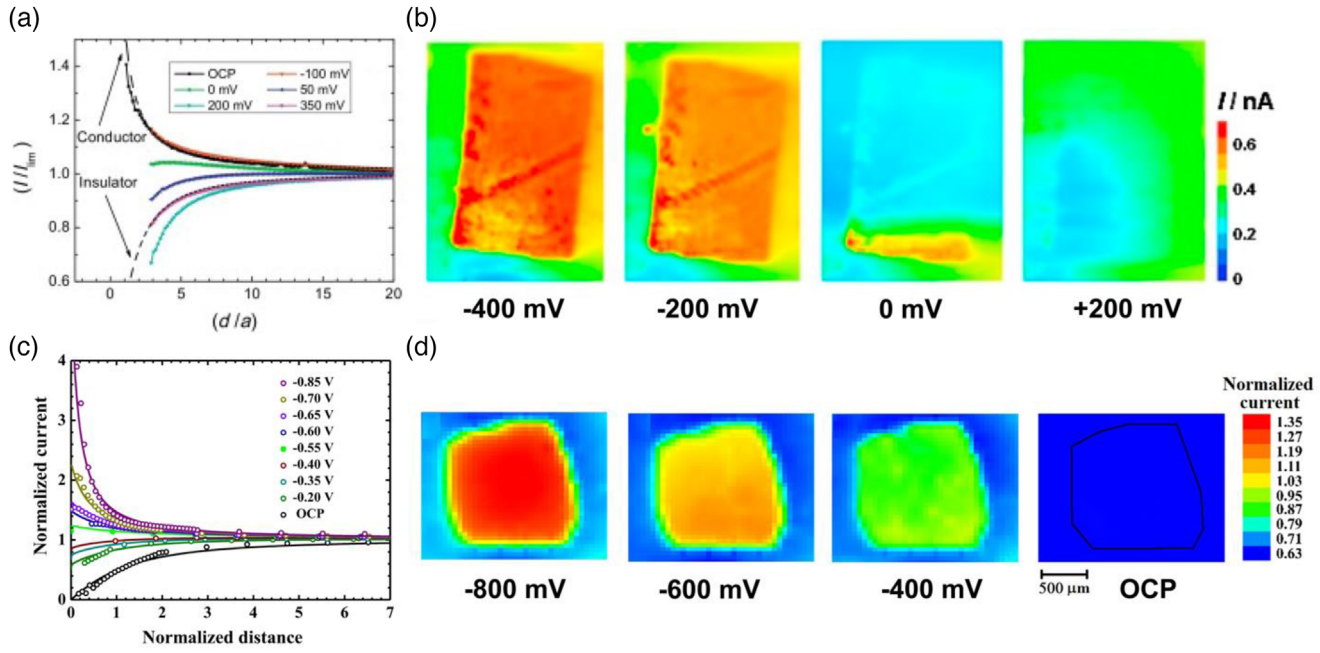

FIGURE 9 (a) SECM approach curves done on a naturally passivated Ti surface at various cathodic potentials applied to the substrate. (b) SECM current maps of the naturally passivated Ti surface at different cathodic potentials applied to the substrate. (c) SECM approach curves done on an anodically passivated Ti surface at various cathodic potentials applied to the substrate, where experimental (symbols) and theoretical (full lines) plots are compared. (d) SECM current maps of the anodically passivated Ti surface at different cathodic potentials applied to the substrate. (A and B) Reprinted from Izquierdo et al.[144] Copyright (2016), with permission from Elsevier. (c and d) Reprinted from Asserghine et al.[174] Copyright (2020) with permission from Elsevier.

film.[175] Care should be taken when comparing studies that utilized different pretreatments, surface preparations, and substrate sources.[172]

3.4.2 | Ti alloys

Ti alloys are categorized into either single-phase (α) or two-phase (α–β) alloys, where the β-phase increases the alloy's strength in comparison with the single-phase alloys.[176] Different grades of Ti alloys include alloying elements such as Mo and Ni (Ti-12), Fe (Ti-2 and Ti-7), Pd (Ti-16 and Ti-7), Al (Ti-5), and Ru (Ti-26 and Ti-27). Some specific Ti alloy compositions have been predominant in the literature, such as Ti_6Al_4V[176] and the near-equiatomic Ti–Ni alloy, nitinol (see Ni section).[138] The resulting passive film's ionic and electronic properties could be heterogeneous due to the different phases and inclusions present in the base metal. SEPM has been useful to understand the effect of intermetallics and/or biphasic structures of the local electrochemical behavior on the passive films on Ti alloys.

The local electrochemical reactivity of Ti-2 alloy (Fe alloying element) was studied using SECM in feedback mode with FcMeOH as the redox mediator (Figure 10).[177] At low concentrations, Fe accumulates in the grain boundaries and triple points of the alloy. Unlike what was previously reported on pure Ti,[173,174] spatially resolved active sites were observed in SECM current maps over an unbiased Ti-2 alloy surface. The sites were proposed to be Fe-rich and located at triple points and grain boundaries (Figure 10b). Similar results were reported for Ti-7 alloy that also contains Fe (and Pd).[178] The authors noted that these active sites are distinguished from those located on pure Ti due to the reactivity at OCP, the higher active site density, and smaller diameters.[177] This could mean that the defects on pure Ti located using SECM were not Fe-rich regions. Approach curves performed at different overpotentials on active and nonactive sites showed variability in the two region's conductivity. As the electrode was polarized toward cathodic potentials, the active sites portrayed an increase in conductivity (Figure 10c), whereas the nonactive sites consistently revealed insulating behavior (Figure 10d). The lack of conductivity measured over the passive films formed on Ti-2 alloy differed from the results obtained over pure Ti during cathodic polarization,[174] albeit more negative potentials were explored in the latter study. It was later shown by the same authors that upon cathodically polarizing Ti-7 to lower potentials the apparent rate constant and the substrate potential was logarithmically related.[178] This increase in rate constant was attributed to the electrochemical reduction of the passive

Review
doi.org/10.1002/elsa.202300014
Chemistry Europe
European Chemical Societies Publishing

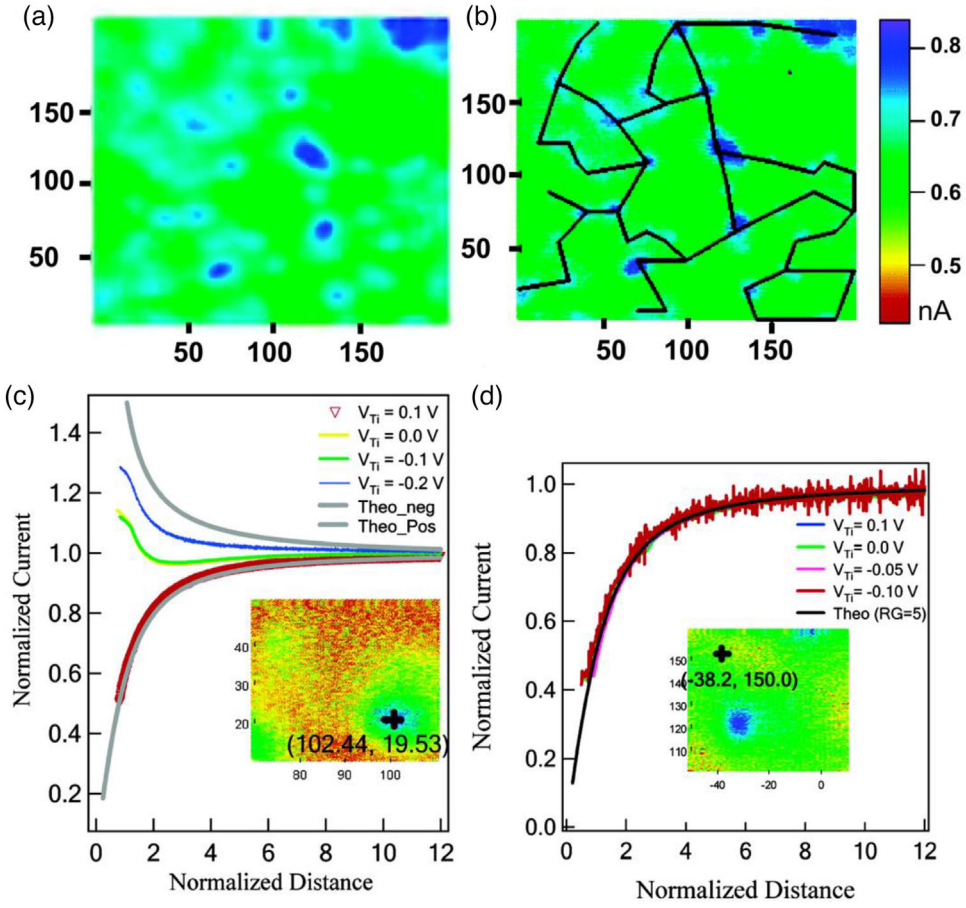

FIGURE 10 (a) SECM current map of Ti-2 sample polarized at 0.00 V versus Ag/AgCl in 0.9 mM FcMeOH solution with 0.1 mmol/L NaCl as the supporting electrolyte. (b) The SECM image with possible grain boundary structures drawn along the Ti-2 surface. (c) Approach curve measurements performed at an electroactive spot on Ti-2 at various applied potentials. (d) Approach curve measurements performed at a nonactive spot on Ti-2 at various applied potentials. Reprinted with permission from Zhu et al.[177] Copyright (2007) American Chemical Society.

TiO_2 film onto the Ti surface to form a more conductive TiOOH layer. It was also found that the rate constant over active sites decreased with an increase in immersion time.[178] This could be due to the accelerated dissolution of the Fe-rich inclusions as a result of forced corrosion via SECM feedback using the redox mediator, FcMeOH (undergoes reduction at the substrate). Ex-situ analysis of the Fe sites after immersion with and without performing SECM measurements would elucidate if accelerated SECM corrosion occurred and whether the Fe inclusions were not protectively passivated by the TiO_2 film to result in local pitting initiation sites.

The naturally formed oxide film on the bi-phasic Ti alloy, Ti_6Al_4V, was interrogated using SECM in feedback mode.[179] It was confirmed by AES that the passive film's elemental composition differed on each phase. SECM imaging clearly revealed a heterogeneous distribution of electrochemical activity along the alloy's surface, which may be due to the difference in oxide composition. However, the current maps were not correlated to the exact location along the substrate's surface using a complementary microscopy method, so the spatially resolved activity could not be confidently assigned to either phase. Regardless, several redox mediators with varying redox potentials were used to investigate the surface kinetics of the oxide layer by recording approach curves over probable single α-phase grains. It was found that, depending on the mediator's redox potential with respect to the energetic position of the oxide's bandgap, the electron-transfer kinetics changed.[179] By varying the applied potential to the alloy, flatband potential values were estimated. Due to the larger UME diameter used, quantitative SECM experiments were not carried out on the β-phase regions as they were much smaller than the UME. Future work on this alloy could involve using a smaller UME to probe the electrochemical activity (conductivity) of both phases, followed by confirmation of the microstructural features using a complementary microscopy technique. In addition, direct and local measurements at different phases could be performed using SECCM. A recent study on

an additive manufactured Ti_6Al_4V used the microdroplet method to investigate the alloy's localized corrosion susceptibility. Using a microdroplet cell with an aperture ~330 μm in diameter (much larger than the α–β-phase regions), the authors showed that the pitting resistance decreased with a higher area ratio of α-phase present.[180] Future studies can take advantage of nanosized pipettes to perform a statistical study on each phase's susceptibility to local breakdown.

3.4.3 | Future work using SEPM on Ti

Most SEPM research efforts on Ti have been focused on probing local defects within the passive film using SECM. While advancements in understanding the nature of the defects located on Ti alloys have been made, the causation of defects found on pure Ti remains unclear. Future efforts should be made to correlate defects on pure Ti passive films to the underlying metal's microstructure. SECCM and correlative studies could also elucidate the influence of grain boundaries and film thickness on breakdown susceptibility. It is clear from the difference in approach curve feedback measurements using different redox mediators on biased Ti electrodes that the passive film is semiconductive. The kinetics of the repassivation of Ti would be interesting to probe in the future. The passive film thickness also seems to play a role in the feedback response obtained. A systematic study exploring the effect of film thickness and feedback response would be beneficial to decouple the effect of ionic and electronic conductivity.

3.5 | Iron

Iron (Fe) is known to have transformed society and is still one of the most important metals to date. For instance, crude steel production alone occurs at a rate of 2.5 million tons annually.[181] Understanding Fe and Fe alloy corrosion mechanisms and inhibition strategies remain at the forefront of research efforts in an attempt to decrease cost and environmental harm.[181]

The observation of passivity was found during the experiments performed by Faraday on Fe in concentrated nitric acid solutions.[17] Potentiodynamic polarization (PDP) measurements in acidic media show that Fe portrays a large dissolution active range, followed by a steep decrease in current density that becomes independent of applied potential (i.e., passive window), which signifies the formation of a protecting passive layer.[14] Although the passive behavior of Fe is not in agreement with what is predicted using thermodynamic data (i.e., Pourbaix diagrams),[182] it is understood that the Fe oxide layers have slow dissolution kinetics.[14] The film (1–5 nm thick)[183–185] consists of an inner magnetite Fe_3O_4 film that is covered by a hematite Fe_2O_3 layer.[184,186] The duplex oxide film behaves like an n-type semiconductor due to defects in the oxide structure, including Fe^{2+} ions in the Fe^{3+} matrix and O^{2-} vacancies. Fe oxides are known to be relatively conductive in comparison with other passive oxide films (bandgap of α-Fe_2O_3 is 1.7 eV).[97] Defects influence the transport through the oxide layer and therefore play an important role in the degradation of Fe.[187] The solution conditions (species present, concentration, pH, temperature)[43] also play a role in Fe passivity, as the metal is protected in concentrated nitric acid solutions,[17] but actively corrodes in neutral NaCl solutions.[188] The effects of solution parameters and microstructural features have been analyzed using SEPM to understand local passivity breakdown and mechanisms.

3.5.1 | Effect of grain orientation on iron passivity

Polycrystalline Fe has been studied to observe the effect of potential,[184,189] pH,[190] and anion concentration[191,192] on its passivation mechanism and kinetics. These studies concluded that both the properties of the oxide and formation rate were influenced by different experimental parameters but did not hold the spatial resolution required to visualize the dependency of passivity on grain orientation. The utilization of SEPM has shed some light on grain passivity behavior, including SECM and SECCM (EDC) measurements.[193]

Fushimi et al.[194] used SECM in feedback mode ($Fe(CN)_6^{4-}$, which undergoes reduction at the substrate) to evaluate the local electrochemical activity of a passivated polycrystalline Fe electrode in pH 8.4 borate solution. The heterogeneity in feedback response was attributed to the difference in passive film thickness over different crystal grains. The probe current was the lowest over the <100> grain orientation, indicating that the thickest passive film formed there.[194] These findings were confirmed in a similar SECM experiment performed in deaerated pH 2.3 sulfate solution.[195]

The EDC method was used to directly measure the influence of grain orientation on the electrochemical behavior of Fe in a pH 6.0 acetate buffer solution.[196] Cyclic voltammetry was performed at many individual grains to measure the local current density and capacitance. In agreement with the SECM studies, it was found that the <100> orientation showed the lowest current density and lowest capacitance (i.e., thickest oxide layer). These observations were confirmed for Fe single crystal samples. Increased corrosion occurred on grain orientations with the most

closely packed crystal faces, whereas oxide formation was preferred on the loosely packed <100> oriented grains.[196] Another EDC study on Fe was performed in sulfuric acid, where different observations were made.[197] It was found that the <100> orientation showed the highest current density and lowest charge transfer resistance value. Complementary XPS studies revealed that the outer hematite oxide was accountable for the protection of the <101> grain at low pH.[197] This may indicate that the oxide properties on different grains are pH-dependent and result in compositional differences.

3.5.2 | Pitting initiation of iron using SECM

The formation of a passive film is a precursor for classical pitting corrosion behavior. It is of interest to probe pitting initiation and propagation spatially using SEPM to gain insight into the mechanisms of action. Studying natural pitting initiation using SECM can be challenging due to pit distribution relative to the size of the microelectrode. To compensate, larger scan areas can be analyzed to increase the probability of detecting pitting events; however, due to the time scale of the experiment (hours), there is the possibility of significant surface film modifications.

As an alternative, SECM has been used to initiate pitting corrosion on Fe.[198,199] These measurements are typically performed using SECM in G/C mode to locally generate Cl^- at the passive film surface. One study found that it was more likely to generate a pit using a larger UME tip since it had a higher probability of covering a grain boundary or a defect site.[199] However, breakdown at arbitrary locations rather than at grain boundaries did occur. Pits were formed at arbitrary locations on a Fe substrate using AFM/SECM by Izquierdo et al.[200] It was found that nitrite ions had a corrosion inhibition effect, but the combination of acidification and high chloride concentrations resulted in a local rapid attack. This study enabled the control of pitting nucleation and the simultaneous imaging of the generated pits using AFM.[200] Although pitting initiation studies using SEPM are useful to predict the probability of film breakdown at different microstructural locations at the material's surface, forcing a pit to nucleate may not be representative of how this process occurs naturally.

3.5.3 | Ferrous alloys: steel

Steels are alloys that mainly contain Fe. Low-cost steels, such as carbon steels, are used as structural components across many industries. Carbon steels contain 1.5% of carbon or less and typically low amounts of Mn, Si, P, and S.[201] The amount of carbon dictates the material's mechanical properties, including strength, ductility, and hardness. Carbon steels can hold a dual-phase microstructure including ferrite and martensite phases, and preferential dissolution of one phase over the other can occur.[202] FeAlCr alloys are lighter alternatives for carbon steel as they hold high formability and deep drawability.[203] These alloys are passive in air and under anodization. Yet, anisotropic dissolution behavior has been observed for these alloys.[204] The presence of microstructural defects and/or features can influence steel's passive behavior which has been resolved by SEPM methods.

3.5.4 | Effect of grain orientation on steel passivity

As with other passivating metals, SECCM studies can provide direct and statistical information about local electrochemical activity. A SECCM study was carried out in sulfuric acid (pH ~2.3) on carbon steel to elucidate the relationship between surface structure/composition and hydrogen evolution reaction (HER) activity.[205] This work exposed a grain orientation dependency for HER activity (with <100> oriented grains being the most reactive) and that this reaction was greatly facilitated by sub-micrometer surface features such as grain boundaries and MnS inclusions. The grain-dependent reactivity was explained through differences in hydrogen adsorption free energy. This study showed an enhancement in the cathodic half-cell process can occur at grain boundaries, potentially fueling intergranular corrosion. This may be due to a difference in passive film characteristics (conductivity, porosity, thickness). Another SECCM study on carbon steel revealed the relationship between anodic metal dissolution during micro-PDP and the crystallographic orientation of low-carbon steel in acidic conditions (Figures 11a–c).[86] The current observed in the passive state was independent of grain orientation (Figure 11d). Once the passive film was removed, the rate of Fe dissolution increased in the order of <101>, <111>, to <100>. The lower rates of dissolution observed on <101> were due to the formation of a corrosion product, or possibly a passive film. However, another SECCM study on carbon steel under neutral conditions (10 mM KNO_3) found that the more densely packed <101> plane was most susceptible to anodic oxidation in comparison with the <100> and <111> orientations.[54] This emphasizes the need to understand local passivity behavior under different solution environments. Although these studies did not focus on passive film characterization over carbon steel, they do provide insight on the reactivity dependence on grain orientation, which will play a role in film formation under different passivating conditions.

Review
doi.org/10.1002/elsa.202300014
Chemistry Europe
European Chemical Societies Publishing

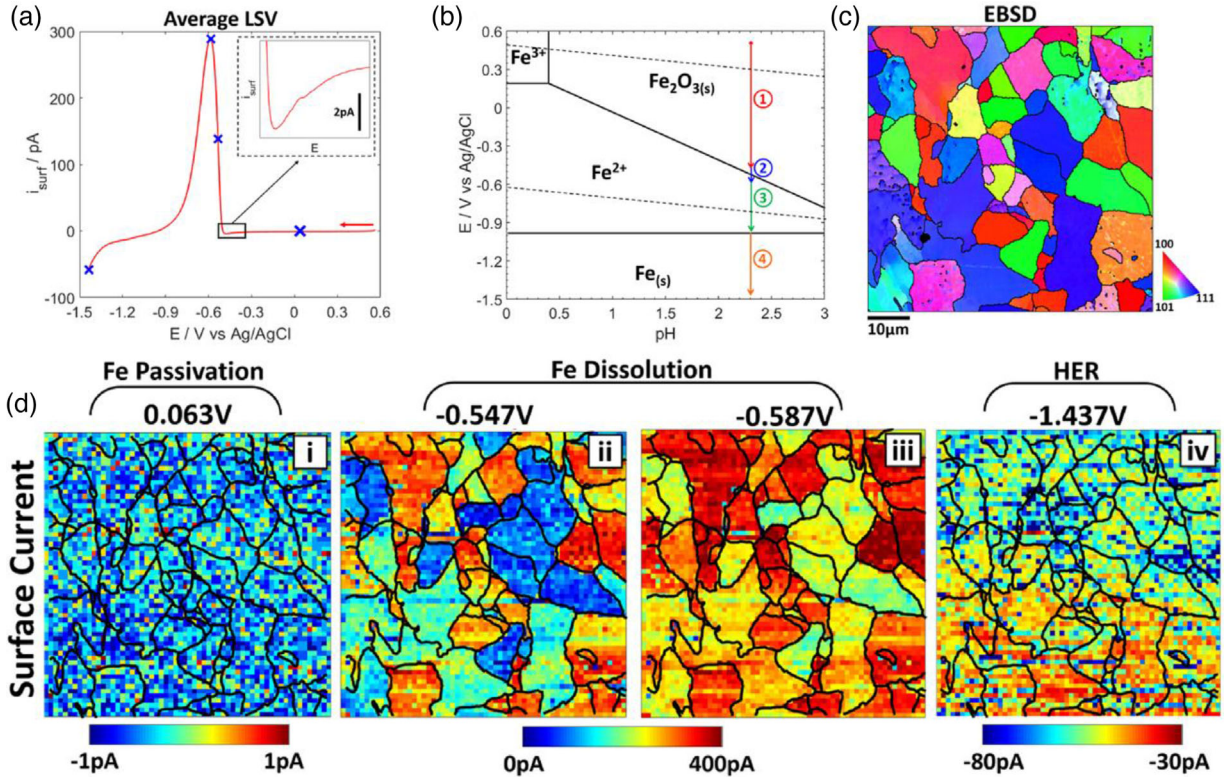

FIGURE 11 (a) The averaged potentiodynamic polarization (PDP) curve obtained from 3600 individual measurements using scanning electrochemical cell microscopy (SECCM) on low carbon steel in 5 mM H_2SO_4. (b) A simplified Pourbaix diagram for Fe, where colored arrows show the potential range covered by the PDP curve in (a) at pH 2.3. The numbers correspond to 1: passive film formation, 2: passive film reduction, 3: active iron dissolution, and 4: cathodic processes. (c) Electron backscatter diffraction maps illustrating the crystallographic structure of the area scanned with SECCM in (d). (d) surface current maps obtained using SECCM for the following potentials (all versus Ag/AgCl): (i) 0.063 V, (ii) −0.587 V, (iii) −0.547 V, and (iv) −1.437 V.[86]

The heterogeneous passivity behavior of dual-phase carbon steel was explored via feedback mode SECM using FcMeOH as the redox mediator.[206] The SECM current map showed a higher film conductivity over the martensitic phase, suggesting that the ferrite phase was more passivated. This could be due to an increase in passive film thickness as suggested by the researchers. This study showed that not only does grain orientation influence passivity, but so does the crystal phase.

The effect of grain orientation for FeAlCr was carried out directly using the EDC method.[204] It was shown that the current density was 53% higher on <100> oriented grains than <111> grains in sulfuric acid. This observation is in agreement with the conclusions drawn from the EDC/SECCM measurements on polycrystalline Fe and carbon steel under similar conditions.[86,197] In contrast, the effect of grain orientation was only found to be marginal for a FeAlCr steel alloy using SECM.[203] While in feedback mode, grain boundaries showed a higher activity, whereas grain faces resulted in lower tip currents. This study suggested that the anisotropic dissolution observed for these alloys was not due to a deficiency in passivation dependent on grain orientation, but from the active dissolution kinetics.[203] Further SECCM investigations using smaller pipettes could provide the statistical evidence needed to clearly identify the effect of orientation on passivity for FeAlCr alloys.

3.5.5 | Passivity breakdown on carbon steel

It has been well documented that the presence of sulfide inclusions such as MnS contributes to the initiation of pitting corrosion in steels due to the interruption of the passive film and their chemical instability.[207–210] This has been validated through the identification of such inclusions and their involvement in the pitting process using SECM using the iodide-triiodide redox couple in feedback mode.[68,211–213] Localized PDP measurements using the EDC method have also confirmed the presence of MnS inclusions during passive film breakdown to form a propagating pit.[78,97] Using SECCM coupled with

structural information, hundreds of micro-PDP measurements have been performed on low-carbon steel to determine the effect of grain orientation and MnS inclusions on electrochemical processes in neutral conditions.[54] The MnS inclusions were found to actively dissolve, followed by the rapid repassivation of the underlying metal matrix. Future SECCM measurements using chloride-containing solutions to study the repassivation kinetics and stability of the film formed in comparison with the natural passive film could elucidate information about the initiation mechanism of pitting at MnS inclusions.

SECM has been used to locally probe the passive response of films on carbon steel in a borate buffer and measure their degradation in NaCl solution.[214] Despite anodic polarization, only negative feedback approach curves were observed using FcMeOH as the redox mediator without NaCl. When NaCl was added to the solution, the SECM current maps showed an increase in normalized tip current, indicating that the films were no long protective in nature.[214] Although SECM was used, correlative microscopy techniques were not employed in this study, so it is difficult to draw conclusions about the influence of defects and their potential heritage. However, this approach may be useful to determine whether the Fe substrate had become passivated.

3.5.6 | Ferrous alloys: stainless steel

Of the alloys available, stainless steels are the second most widely used materials after carbon steels because they are corrosion resistant, tough, hygienic, castable, and have long life spans—making them suitable for a wide range of applications.[215] The large number of alloying elements used to enhance certain properties of stainless steels makes for a larger possible range of crystal structures and intermetallic phases. The three main types of stainless steels are ferrite (bcc),[216] austenite (fcc),[217] and martensite (fct),[218] which form depending on the alloying elements (i.e., Ni in austenite) included and processes parameters (i.e., cooling rates) used. In contrast to carbon steels, stainless steels contain no less than 10.5 wt% chromium.[219] The chromium content is crucial for their corrosion-resistant behavior—it oxidizes in air to form a very thin (nanometers)[31] chromium oxide film that protects the underlying metal from further degradation. The conductivity of Cr-rich passive films differs from Fe-rich passive films (bandgap of Cr_2O_3 is 3.5 eV).[28] Deterioration or damage to this passive film causes detrimental localized corrosion processes to occur, where exposure of the vulnerable underlying material can lead to intergranular and pitting corrosion.

3.5.7 | Passivity breakdown of stainless steel

SECM has been used to study the breakdown of passive films on stainless steels in an attempt to understand its pitting initiation and propagation mechanisms. The in situ characterization of meta stable pitting has been reported on stainless steels using SECM in feedback mode[220] and G/C mode.[221] Pit formation on stainless steels has also been forced using G/C mode.[60] AC-SECM was used to visualize very small corrosion pits before and after pit initiation to identify the region of broken passivity.[77]

LEIS mapping has been used at a single frequency to locate pitting events on Fe–Cr alloys.[222] It was found that the solution resistance decreased in the region around the pit and that LEIS could provide insight into pitting initiation and propagation. LEIS was also utilized to study the effect of Mo as an alloying agent in Fe–Cr alloys and provided localized kinetic information about stages in pit growth.[223] The influence of Mo was repassivation at the early stages of pitting and the enhanced formation of a salt film (or possibly a passive) layer. It was hypothesized that the salt film was present as a duplex structure, but better resolution in the high-frequency region would be necessary to draw such conclusions.[223]

More recently, SECCM has been used to probe the stochastic nature of passive film breakdown (i.e., pitting).[224] Over one thousand micro-PDP measurements were performed on stainless steel 316L. At potential regions before passivity breakdown, the current density portrayed a unimodal distribution, whereas a uniform distribution was observed at potentials related to stable pitting.[224] The uniform distribution confirmed that pitting corrosion occurs with a high degree of uncertainty, which increased with chloride concentration and decreased with scan rate. This study demonstrates the advantage of using SECCM to statistically probe passive film breakdown behavior. Future studies to obtain identical location correlation of SECCM footprints with surface analysis will hold exciting information about the influence of microstructural features on passivity breakdown.

3.5.8 | Effect of inclusions on stainless steel passivity

Localized damage to stainless steels has been extensively linked to intermetallic phases formed with other alloying elements within the Fe–Cr matrix.[225] This is because the intermetallic phases have differing chemical/electrochemical properties than the surrounding metal matrix, which can result in either chemical dissolution or the formation of a local galvanic couple. SEPM methods

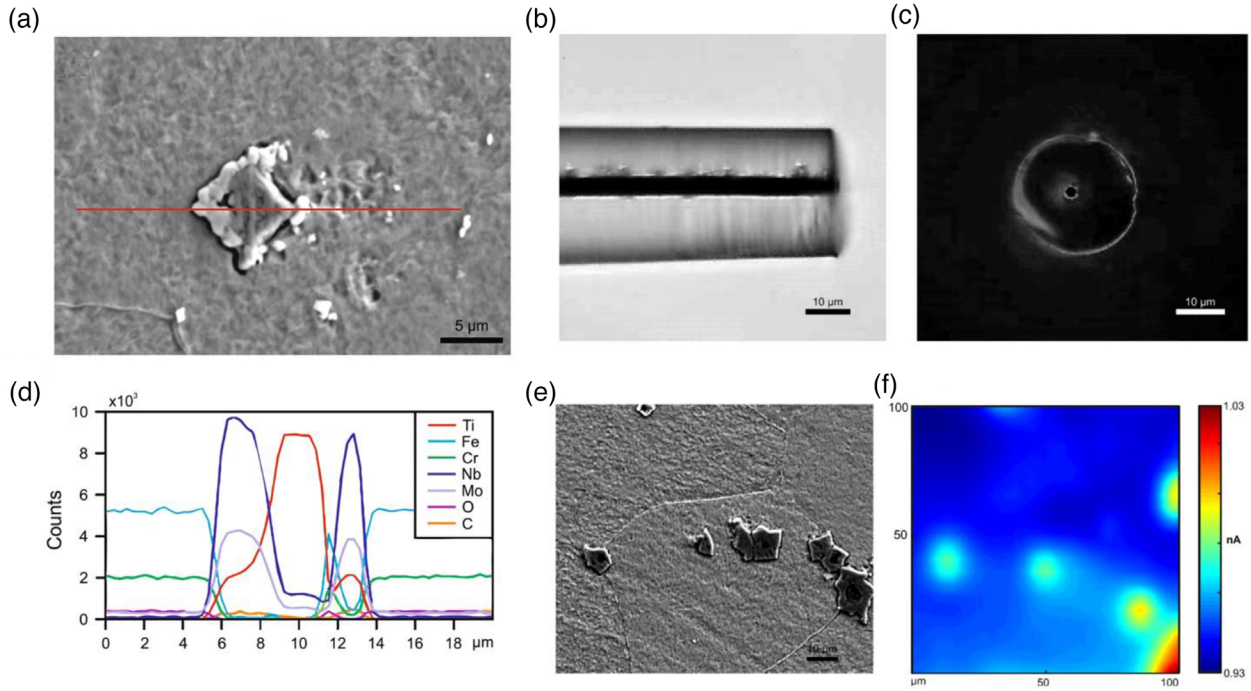

FIGURE 12 (a) Scanning electron microscope (SEM) image of a TiN inclusion after a macroscale potentiodynamic polarization measurement in an etching solution, showing the resulting localized corrosion adjacent the inclusion. (b) The side view and (c) top view of the carbon fiber ultra microelectrode used in scanning electrocehmical microscopy (SECM) measurements over stainless steel 444. (d) Corresponds to the energy-dispersive X-ray spectroscopy linescan across the TiN inclusion in (a). (e) The SEM image and (f) current map obtained using SECM of similar sites on the substrate, indicating that the local hotspots detected correspond to the conductive inclusions within the material's microstructure.[59] http://creativecommons.org/licenses/by/4.0/.

are useful for probing the local electrochemical activity of these phases to reveal their passive nature, or lack thereof.

In addition to steels, the presence of MnS inclusions is parasitic for initiating localized corrosion on stainless steels.[53,212,208,226–228] Much work has utilized the EDC method to observe the effect of MnS inclusion size, distribution, and electrolyte composition/concentration on the repassivation behavior of the underlying metal after MnS dissolution. It was shown that fast repassivation was achieved for nanosized MnS inclusions on steel.[54] A future SECCM study on steel and stainless steel materials with MnS inclusions would be interesting to compare their repassivation rates.

The precipitation of Cr with parasitic amounts of carbon ($Cr_{23}C_6$) leads to Cr-depleted regions vulnerable to intergranular corrosion attack.[229] Using the EDC method, micro-PDP measurements confirmed that regions adjacent to Cr-rich inclusions are the weakest areas leading to localized attack.[230] This may be due to this region's lack of repassivation capability. The elimination and/or minimization of Cr-rich inclusions in stainless steels is desired to avoid failure during repassivation attempts.

One method for inhibiting $Cr_{23}C_6$ formation is the use of stabilizing alloy elements such as Ti and Nb to form Ti- and Nb-rich carbide/nitride inclusions (Figures 12a and d). The effect of Ti and Nb-rich inclusions on stainless steel corrosion resistance was explored using SECM in feedback mode (FcMeOH redox mediator) while utilizing a 7 µm carbon fiber UME (Figures 12b and c).[59] The inclusions were electrochemically reactive, as seen by the observed positive feedback hotspots measured using SECM and correlative SEM imaging (Figures 12e and f). The passive film over the metal matrix was insulating, confirmed by a negative feedback SECM response. The stability of the inclusions and passive film during long-term immersion was confirmed using SECM current maps. This study showed that the inclusions were either not passivated or portrayed different passive film properties (conductivity and/or thickness) than the metal matrix passive film. Further, the electrochemical stability of the inclusions was demonstrated using macro-PDP measurements in acidic solutions. This study suggested that the inclusions were exposed to facilitate the reduction of oxidizing species and promote the localized corrosion of the adjacent metal matrix through a microgalvanic coupling mechanism.[59]

SEPM techniques have also been applied to newly developed stainless steel coating fabrication methods.[231] Using SECM in feedback mode (FcMeOH), the lack of passive film formation on thermally sprayed stainless steel 444 was evident by the positive feedback response at OCP.[231]

Micro-PDP measurements were performed on a single stainless steel 444 particle (used as the precursor material to fabricate the coatings) and active corrosion behavior was observed. This confirmed that the removal of passivity was due to the powder fabrication process.

3.5.9 | Effect of mechanical stress on stainless steel passive films

The synergy between passivity and tensile stress can result in stress corrosion cracking while immersed in a corrosive environment.[232] Questions remain about the formation and growth mechanisms of a crack. Changes in the oxide film coverage may occur when grain stretching is induced by the application of tensile stress. Nanoscale and microscale techniques have been of use to study the effect of mechanical strain on local electrochemical activity.[233]

Using hexaammineruthenium for SECM in feedback mode ($Ru(NH_3)_6^{3+}$, which undergoes oxidation at the substrate), the change in the kinetic rate constant while applying tensile stress to T-316 stainless steel sample was explored.[234] The rate decreased with increasing tensile stress, which was counterintuitive to the hypothesis that the disruption of the passive film would reveal fresh (not passivated) metal that would increase the rate. It was mentioned in this study that the rates measured varied significantly between different points on the same sample. SECM was used to investigate the effect of mechanical stress on the local passive film behavior of stainless steel 304L.[235] Sidane et al.[235] used ferricyanide ($Fe(CN)_6^{3-}$ undergoes reduction at the substrate) and showed that its kinetic rate constant increased with increasing stress strength. This was attributed to the acceleration of the transport of oxygen vacancies according to the point defect model (PDM).[235] Similar findings were reported for alloy 800 (Ni Cr stainless steel) under tensile and compression stress.[236] This study used FcMeOH (undergoes reduction at the substrate) to probe localized surface reactivity in thiosulfate-containing solutions, indicating that mediators that undergo reduction at the metal surface can be useful for probing passivity changes for stainless steels under stress/strain. The contradicting results found in Sun et al.'s studies were probably due to the difference in chemical composition (electronic properties) of the passive films, or the use of a mediator that undergoes oxidation (i.e., induces metal reduction).

LEIS was used to study the changes in capacitance of the passivated 301 NL stainless steel in borate electrolytes.[237] It was found that strain increased the capacitance and decreased the material's ability to repassivate, suggesting that the dislocations created defective (and not protective) oxide films. The spatial resolution was on the order of millimeters, and therefore information about how microstructural features influenced the changes in capacitance was not realized.

The EDC method has also been used to implement local electrochemical methods to evaluate the effect of stress on stainless steels.[238–240] Stainless steel 304 was found to undergo a discontinuous process and active and passive phases during crack growth and was explained by the film rupture model.[240] It was later shown that the level of Cr content in 304 influenced the effect of stress when exposed to high levels of chloride.[239] The presence of microstructural features also revealed a synergistic effect on crack initiation for alloy 718.[238] Advanced SECCM studies on SCC and passivity would be useful to understand the direct correlation with microstructure, passivity, and cracking mechanisms.

3.5.10 | Future of SEPM on iron and ferrous alloys

It is known that Fe oxide passive films are easily reduced onto the meal surface upon cathodic polarization.[183,241] This is because the oxides are relatively conductive in comparison with other passive films. Future work involving SECM could be investigating the effect of repassivation after oxide reduction to observe the kinetics of film formation. Most SECM studies on Fe and alloys are done in feedback mode, specifically using a redox mediator that undergoes reduction at the substrate, which can induce oxidative etching. Other redox mediators should be used to probe the passive film's conductivity and eliminate the possibility of etching. Although pitting initiation studies have been performed, these works do not conclude the effect of microstructural features and defects. It is clear from SECM studies using feedback mode that passive films on inclusions differ from the films formed on the metal matrix, which are vulnerable sites for local breakdown. A systematic study of film breakdown using SECM in G/C mode at different regions along the substrate would be interesting to gain statistical insight on film breakdown susceptibility, particularly in chloride-containing solutions. Many studies using SECM, EDC, and SECCM have investigated the influence of grain orientation on passive film properties for pure Fe and steels, yet there remains a gap in the literature using such methods on stainless steels. Future SECCM studies with correlative microscopy methods could provide direct and local information about how/if passive film properties change on microstructural features. Last, information about repassivity capability for all Fe-based materials would be beneficial to understand the

material's ability to passivate after physical and/or chemical damage.[242]

3.6 | Copper

Copper is a noble metal that is often used as a corrosion-resistant material for high-performance applications such as nuclear waste containers,[243,244] antimicrobial surfaces,[245,246] and intrauterine devices.[247,248] However, passivity is a prerequisite for Cu's performance under highly corrosive environments to ensure a slow corrosion rate. At high pH, Cu is susceptible to localized corrosion (i.e., pitting and crevice corrosion). The passivation capability of Cu and its film protectiveness is a topic of debate,[249–251] but generally is considered to form under alkaline and neutral conditions and in the presence of sulfide.[252,253] The semiconductive film (bandgap 1.7 eV)[97] is a duplex layered structure (10 nm thick) consisting of a Cu_2O/Cu(OH)-layer on top of a thin layer of CuO over the metal.[254] Surface roughening (nonuniform corrosion) of Cu has been observed[243] and pit formation has been observed under anodic polarization.[255] An understanding of the difference between mechanisms for roughening and classical localized corrosion has not been clarified. Local electrochemical techniques have been employed to study the passivation and corrosion behavior of Cu to uncover its mechanism of localized corrosion.

3.6.1 | Probing the etching kinetics of different redox mediators

Macpherson et al.[256] studied the oxidative etching of unbiased Cu in sulfuric acid using in situ generated Br_2 and $Ru(bipy)^{3+}$ and found that these redox mediators etch Cu under diffusion-limited conditions. The study deconvoluted conductivity and etching kinetics by reducing the size of the Cu to a comparable size to the microelectrode. In this way, the rate constant of Cu etching was estimated to be a minimum value of 0.4 cm/s. Similar results were reported earlier for Mandler and Bard[257] using $Fe(phen)_3$ and $Os(bpy)_3$ in 10 mM Acetate buffer for surface patterning purposes. These findings demonstrate the high reactivity of Cu in the feedback mode, presumably due to the high conductivity of Cu and/or the Cu oxide film, and that mediator interactions are important considerations when investigating a corroding material using SECM. Similarly, the dissolution of Cu and the following detections of Cu^{2+} species has been performed with AFM/SECM and AC-SECM under nonpassivating conditions.[258]

3.6.2 | Evaluating of the effect of grain orientation on copper passivity

Intrinsic differences in the behavior of different grain orientations can induce microgalvanic coupling effects, influencing corrosion and passivation behavior. Martinez-Lombardia et al.[259] studied passivated and nonpassivated polycrystalline Cu using correlative EBSD and SECM in orthophosphate buffer (pH 12). The authors showed a grain orientation dependency on passivation, where there is a thicker, more passivating, oxide layer was formed on <111> oriented grains (Figures 13a and b). In nonpassivating conditions and contrary to predictions based on surface energy and work functions, the highest corrosion rate was observed on <111> oriented grains.[259] The authors also report some heterogeneity in the passive film and that the grain orientation of neighboring grains influences the passivation and corrosion rate. Yet, the precise influence of etching versus conductivity effects for these SECM measurements using FcMeOH in this study remains unresolved, and an improved understanding of the influence of FcMeOH on Cu corrosion can help clarify these results in the future.

SECCM studies are highly advantageous to investigate grain orientation effects as they can measure the direct electrochemical behavior without an externally added mediator. SECCM studies on Cu in carbonate buffered conditions have revealed direct measurements of the cathodic processes occurring on polycrystalline Cu (Figures 13c and D).[260] Under deaerated conditions, the authors reported a lower reduction potential for $Cu(OH)_2$ on <100> than <111> oriented grains, which supports the passivation effects found by Martinez-Lombardia et al.[259] Yet, more knowledge is needed to fully unravel the grain orientation-dependent passivation of Cu under different corrosion-related conditions, as the study was predominantly interested in electrocatalytic conditions. Recently, the effect of Cu crystallographic orientation on corrosion inhibition has been evaluated under acidic conditions,[261] but such conditions do not represent passivating conditions. One drawback of SECCM measurements is that the influence of nearby grains for potential galvanic coupling is removed.

3.6.3 | Copper alloys

Cu alloys are frequently encountered in our society. Brass is a commonly used Cu alloy (Zn additive) in cooling water applications for heat exchangers.[262] Dealloying of brass in acidic environments indicates its lack of passivity.[263] On the other hand, bronze statues (Sn additive) have been

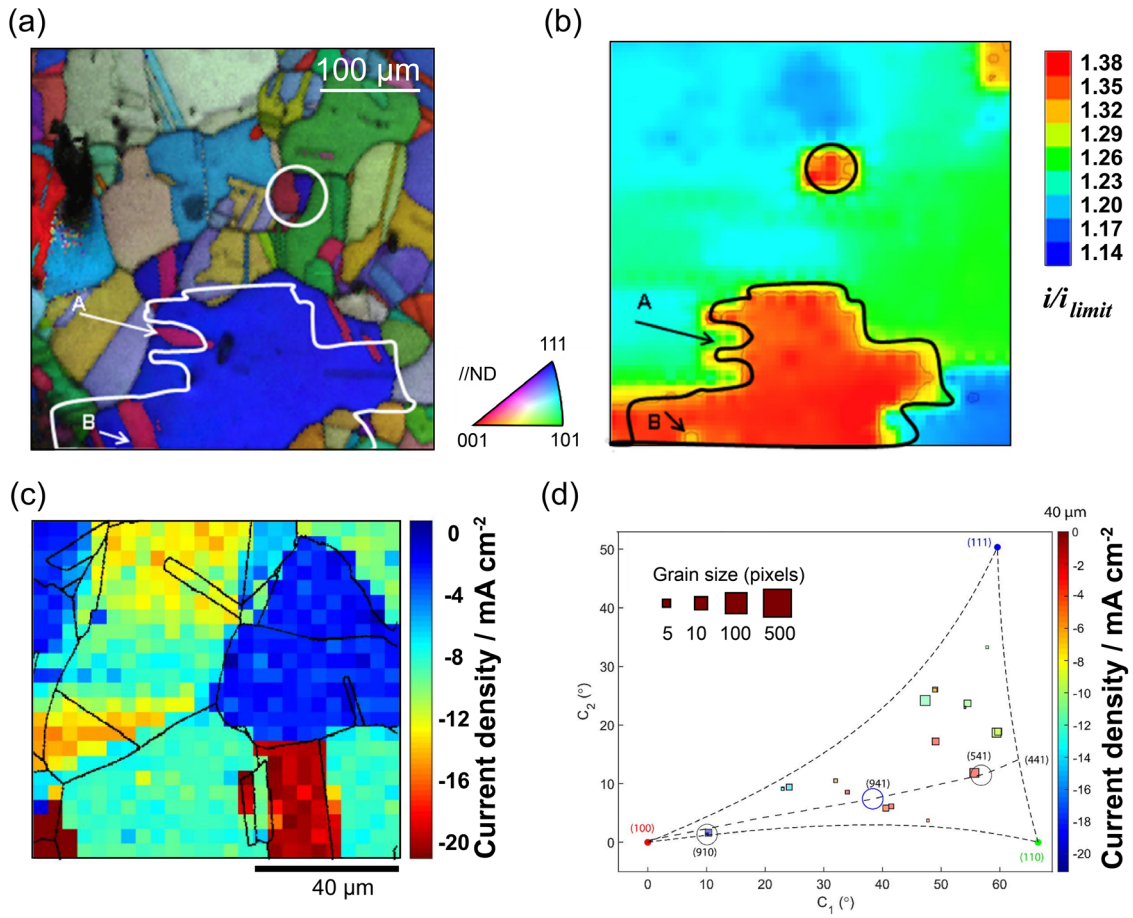

FIGURE 13 (a) Inverse pole figure/image quality map of polycrystalline copper. (b) Corresponding scanning electrochemical microscopy current map (400 × 400 µm) in sodium hydrogen orthophosphate/sodium hydroxide buffer solution with 5 mM ferrocenemethanol. (c) Current image at $E_{surf} = -1.05$ V versus Ag/AgCl with a nanopipette filled with 10 mM $KHCO_3$ under Ar-purged conditions.260 (d) Correlated electrochemical data with corresponding 2D projection of Cu grain orientations.[260] (a and b) Reprinted from Martinez-Lombardia et al.[259] Copyright (2014) with permission from Elsevier.

preserved all over the world for thousands of years, indicating the protective nature of the passive film formed.[264] Guadagnini et al.[265] studied a quaternary bronze material under acidic and neutral conditions using FcMeOH. The study revealed heterogeneous electrochemical behavior of the alloy and correlative SEM/EDX analysis showed that some regions formed corrosion product on the surface, which was mainly Sn and Cu oxides. Their different conductivities resulted in increased corrosion rates. The study also clearly presented the effect of immersion time to show that passivation of the bronze surface occurs after about 24 h, demonstrating that passivity is a slow process on this Cu alloy.[265]

3.6.4 | Future work using SEPM on copper

SECM and SECCM have been applied to study local passivation at different grain orientations of copper. Yet, mechanistic insight into the local passivation breakdown has not yet been studied by SECM or SECCM, and more work is needed to fully understand the effect of grain orientations on bulk corrosion properties. Systematic studies of the influence of different redox mediators are needed for improved interpretation of SECM results, where mediators that undergo oxidation at the substrate might be more effective to avoid Cu etching. As demonstrated by the study on bronze,[265] the degradation of Cu alloys is also another important future work as intermetallic particles can serve as corrosion initiation sites for passive film breakdown and/or galvanic coupling. The combined identification and localization and investigation of the electrochemical behavior of such intermetallic particles can provide new insight into the passive film breakdown. Similarly. SECM and SECCM can be used for studying advanced Cu materials such as cold spray Cu coatings that display highly heterogeneous particle-particle boundaries, whose precise role in corrosion is still under investigation.[266]

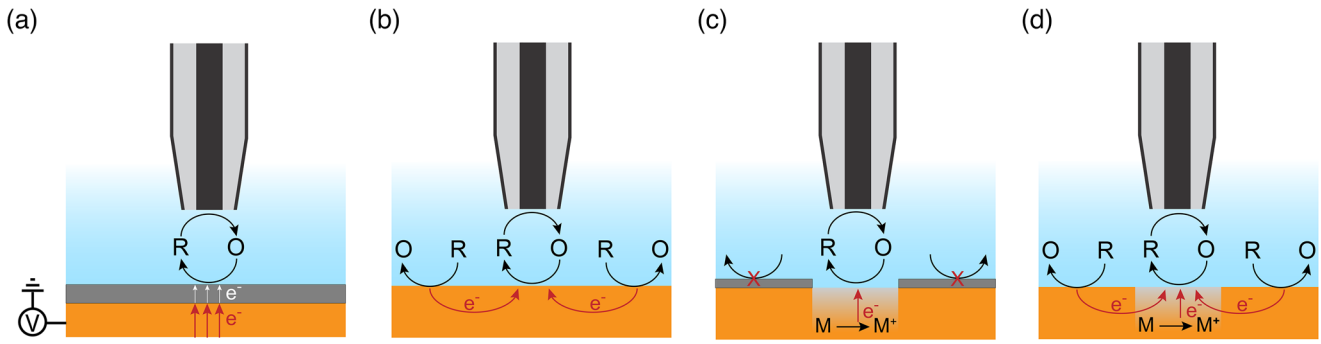

FIGURE 14 Mechanism for redox mediator generation in scanning electrochemical microscopy feedback mode. (a) tunelling through a thin oxide film on a polarized metal substrate. (b) Conductivity effects only, where the redox mediator in solution controls the substrate potential such that the tip reaction occurs at the substrate away from the diffusion field of the microelectrode. (c) Etching of the substrate by the redox mediator formed at the microelectrode. (d) Combined etching and conductivity effects.

4 | STATUS OF THE CURRENT LITERATURE AND PROMISING FUTURE AVENUES

The following section focuses on summarizing and discussing the limitations of SEPM in passivating corrosion studies, potential improvements needed to quantify passivity parameters, and future uses of SEPM in studying advanced passive materials and films.

4.1 | Limitations of the SECM feedback mode

When carrying out SECM in feedback mode over passivated regions on polarized conductive metals, the redox activity probed reflects the local rate of electron tunneling across the oxide film and/or the electronic conductivity of the film (Figure 14a). A local higher electronic conductivity observed in SECM current maps may be a redox-active site that corresponds to a structural or electronic defect site within the passive film. However, depending on the redox mediator employed, SECM feedback mode measurements may induce accelerated corrosion, particularly when the substrate is at OCP. At OCP, the redox mediator regeneration at a conductive substrate is generally considered to be sustained by the opposite reaction somwhere else on the surface (Figure 14b). However, mediators that undergo reduction at a conductive, corroding substrate can instigate substrate oxidation (corrosion) to generate the electronic charge needed to reduce the mediator to complete the feedback loop (Figure 14c). Accelerated substrate corrosion, or oxidative etching, can occur throughout the collection of a SECM current map and during approach curve measurements.[256] This has been seen for nonpassivating metals such as Mg,[267,268] as well as metals under nonpassivating conditions including Cu[256] and ferrous coatings.[231]

It is difficult to differentiate between oxidative etching and conductivity while only employing a redox mediator that undergoes reduction at the substrate and using relatively fast scan rates, where a combined effect may result (Figure 14d).[269] The occurrence of oxidative etching would infer that the oxide film is not protecting the underlying material from further degradation. Hence, it is a good indication of whether the oxide film is passive or nonprotective in nature. Oxidative etching may occur locally over passivated metals that contain exposed (i.e., not covered in a passive film) electrochemically active inclusions. If the inclusion is of the same dimension as the UME and the surrounding metal is completely covered in a fully passivating film, the substrate's potential-driven feedback is negligible, and the response measured at the UME is solely the etching kinetics of the inclusion.[256] If these inclusions are conductive and inert to anodic dissolution, the heterogeneous rate constant will only be measured when the substrate is externally polarized. If inclusions are electrochemically active at OCP, the current has to be sustained by electrochemical processes on other inclusions or through the passive film. A way to determine whether positive feedback is generated from oxidative etching or local conductivity is by using different redox mediators that reduce or oxidize at the substrate. If positive feedback is measured with both mediators, then local conductive features have been identified. Care should be taken when interpreting the SECM response of a metal that undergoes oxidative etching. For example, topographical changes due to etching can occur and SECM is sensitive to the tip-to-substrate distance. There can also be complex intermediate and product speciation that can be detected at the tip. Last, the precipitation of corrosion products can interfere with the true behaviour of the metal.

Review
doi.org/10.1002/elsa.202300014

Despite its popularity, the feedback mode of SECM indirectly monitors corrosion kinetics due to the reliance on a redox mediator, thus requiring the probe's response to remain stable for the entire measurement. The addition of a redox species in the test solution can alter the substrate's OCP and impose unwanted electrochemical reactions.[52] Of the redox mediators used to probe passive metals, FcMeOH is by far the most readily used. It has been rendered to be useful for detecting heterogeneity in passive films, including local defect sites. However, this mediator is reduced at the substrate's surface, meaning that it may induce oxidative etching. Electrochemical reduction of the passive film by redox mediators that undergo oxidation at the substrate surface is also a possibility under certain conditions. To fully understand the feedback mechanism of SECM on a passive material, a redox mediator screening study should be done using species that undergo both oxidation and reduction at the substrate. This should be followed by ex-situ microscopy analysis to investigate the defect sites (inclusions) before and after SECM studies to check for signs of accelerated dissolution.

4.2 | Deconvoluting topography and reactivity

SECM is also sensitive to topographical features, where changes in corrosion film thickness and localized corrosion regions (i.e., pits) can result in surface roughening and hence difficulties in interpreting the current response in SECM maps quantitatively. Feedback mode required the tip-to-substrate distance to be known, which is often estimated by making contact between the microelectrode and the surface from approach curves. Quantitative imaging is highly desired to make full use of the spatial resolution of SECM. The negative and positive feedback behavior is quantitatively related to the tip-substrate distance. Typically, embedding the metal in insulating epoxy, polishing the surface flat, and imaging the whole sample with the negative feedback regions is the most common way to solve this problem.[256] The tip-to-substrate distance is then calculated from the current over the substrate. This problem can also be solved for a conductive sample when polarized to give positive feedback.[65] The most accurate way of performing this analysis is to extrapolate the negative feedback current and fit each point of the image for an apparent normalized tip-to-substrate distance and use this value to fit for the kinetic rate constant, a method referred to as quantitative feedback referencing.[65] More complex methods based on technique hyphenation allow for reactivity/topography deconvolution over the passive film itself, which is important for future reactivity/topography deconvolution on the nanoscale.

4.3 | Quantifying passive film parameters using SECM

The varying feedback behavior measured over Ti suggests that the passive nature of the film may be determined by its thickness and porosity. One advantage of SECM is the technique's potential to probe passive film parameters in situ. Most SECM studies on pores have been done on membranes with pore dimensions larger than, or similar to, the UME used.[270,271] Based on the SEPM studies reviewed herein, many passive film defects are smaller than a typical UME size (10–25 μm).[90] Thus, information about film discontinuity due to defects could be realized by utilizing SECM to extract film porosity.

The quantitative extraction of film thickness and porosity has been done for insulating passive films on reactive metals using SECM approach curve measurements and applying finite elemental modeling.[272] The porous layer was accounted for by modifying the SECM analytical expressions for approach curve measurements. Experimental approach curves were measured on commercially available insulating porous films over a conductive substrate. By fitting the results to the modified expressions, a good agreement between the commercial source values of porosity and thickness was obtained. This approach could be used on insulating passive films, such as Al_2O_3 and ZrO_2, and compared with complementary techniques like EIS and XPS for validation. Unlike EIS and XPS, SECM may be a method to locally probe passive film parameters in the future to better understand the relationship between thickness, porosity, microstructure, and local breakdown events. Complementary microscopy methods would enable the correlation of local electrochemical responses with nanostructural and microstructural features of the passive film and underlying metal.

4.4 | Decoupling ionic and electronic conductivity of passive films

Many SECM studies on passive films focused on measuring film electrical conductivity via the local charge transfer rates, detecting local defects along the film's surface, and intentionally forcing the pitting of the underlying substrate by local film breakdown. In addition to quantifying the electrical conductivity of a passive film, the ionic conductivity within the passive film can contribute to the measured properties and corrosion behavior.[234] Ionic conductivity within a passive film is modulated by the ionic distribution within the porous film due to electric double layer effects, where cation depletion and anion accumulations occur or vice versa, depending on the charge of the passive layer. As a result, the mass-transport

Review
doi.org/10.1002/elsa.202300014
Chemistry Europe
European Chemical Societies Publishing

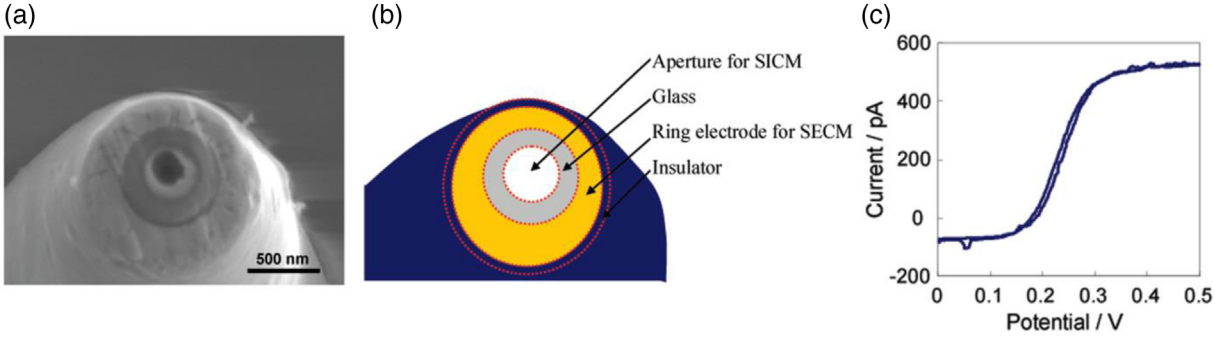

FIGURE 15 (a) Scanning electron microscopy (SEM) image of the scanning electrochemical microscopy/scanning ion conductance microscopy (SECM/SICM) probe and (b) a schematic representation of the probe structure. (c) The cyclic voltammetry response of the SECM ring electrode in 0.50 mM ferrocenemethanol and 0.1 M KCl at a scan rate of 100 mV/s. Reprinted with permission from Takahashi et al.[279] Copyright (2010) American Chemical Society.

and electron transfer kinetics are altered,[273] which can be critical for film growth and possibly film breakdown initiation and propagation mechanisms.[1] The convoluted contributions of both electrical and ionic conductivity of semiconducting passive films make it difficult to extract localized information about mass transport through the film. This is especially difficult to decouple for ultrathin semiconductive films (<2 nm) that enable tunneling to the conductive substrate as well. Further complications in SECM studies arise when the passive film thickness is dynamic (i.e., has not reached a steady state).[274] Alternatively, SICM could be employed. SICM has been readily employed to map surface topography[275] and more recently to image surface charge and ion conductivity on the nanoscale.[276–278] Moreover, SICM can be used to locally polarize the sample without a mediator to induce passivity breakdown. SICM has yet to be harnessed in corrosion studies. Future research involving SICM to measure the ionic conductivity of passive films could be beneficial. Interestingly, the combination of SECM and SICM has been reported for simultaneous topography and electrochemical imaging (Figure 15).[279] Nanoring electrodes were fabricated by depositing Au onto nanopipettes to realize the dual imaging technique (Figures 15a and b), which gave good steady-state behavior (Figure 15c).[279,280] A similar probe geometry could be used to simultaneously extract electronic and ionic conductivity over passive films to advance the scientific community's knowledge of each conductive pathway's influence on film growth and breakdown mechanisms.

4.5 | Direct and local electrochemical impedance measurements using SECCM

Although the drive to use LEIS stemmed from the desire to investigate the influence of inclusions, grain boundaries, and other surface heterogeneities on localized corrosion, such studies are difficult to realize due to the technique's lack of spatial resolution (order of a few micrometers).[72] A future avenue to improve LEIS resolution is the fabrication and utilization of smaller electrodes. Furthermore, until recently, the radial contribution to the current density has been neglected in LEIS measurements using dual-probes due to the assumption that the normal current component is predominant. This stems from the original study's use of large (millimeters) dual-probes to study large samples.[72,91] Considering the highly localized nature of passive film defects, both the radial and normal contributions to the electric field should be measured using the recently developed tri-microelectrode probe.[73] The AC-SECM mode has been successfully used to measure the local impedance of a passive film-covered substrate with higher spatial resolution than LEIS, yet the method also holds some drawbacks. The quantitative analysis of the experimental data can be difficult since the response is both tip/sample local intrinsic capacitance ratio and frequency dependent.[61]

Alternatively, LEIS measurements can be directly applied to localized regions by implementing SECCM.[82] The combined LEIS-SECCM method improves the spatial resolution (~180 nm) of LEIS and enables the direct measurement of the interfacial electrochemical behaviors of materials. Considering the advancements made in understanding corrosion science and passivity using EIS,[38,154,281,282] the direct application of LEIS at the microscale and nanoscale using SECCM holds great promise. There is potential to locally identify and quantify the bilayer structure using LEIS through fitting experimental data to model circuits. Local charge transfer resistance, film capacitance, and film thickness could be imaged on individual grain orientations, boundaries, and inclusions to answer the remaining questions about these parameters on passive film properties and behavior.

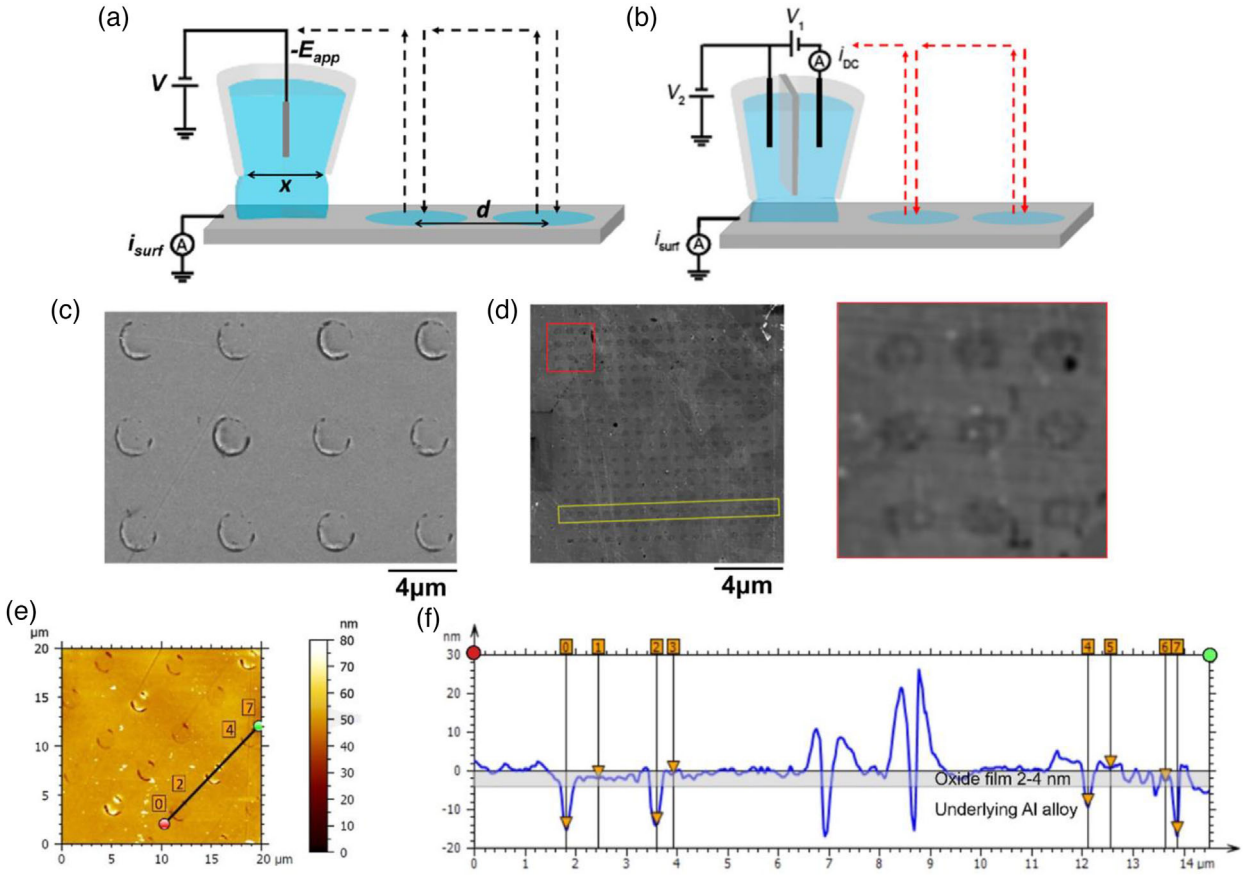

FIGURE 16 Schematic representation of (a) a single barrel[205] and (b) dual-barrel scanning electrochemical cell microscopy (SECCM) setup that enables spatially resolved electrochemical measurements to be realized.54 The arrows show the probe path in a hopping mode. (c) Scanning electron microscopy (SEM) image of the SECCM scanned Al alloy surface after measurements, where indentations can be seen by the pipette landings while using a single-channel pipette. (d) SEM image of the droplet footprints made on low-carbon steel after SECCM measurements performed using a dual-channel pipette.[54] (e) Shows the atomic force microscopy image and (f) topography line scan across the indentations made using a single-channel pipette. (c, e, and f) Reprinted with permission from Li et al.[285] Copyright (2022) American Chemical Society.

4.6 | Dual-channel SECCM probes for future passivity studies

The use of SECCM and complementary microscopy in corrosion science has already begun to advance the community's knowledge about how surface structural factors influence the local stability of a metal. Unlike EDC measurements, thousands of localized experiments can be carried out within a laboratory-friendly time scale to provide statistically relevant information at different sites along a corroding metal's surface.[86,112,224]

For most SECCM corrosion studies to date, single-channel pipettes have been used to form the microelectrochemical or nanoelectrochemical cell (Figure 16a). The feedback method (i.e., surface current) to locate the position of the single-channel probe requires that the substrate is conductive.[283,284] For nonpassivating metals or semiconducting films, the feedback method has been used successfully. However, in the case of using SECCM to study metals with insulating passive films (Al, Zr), the use of single-channel pipettes requires that the substrate is polarized to high overpotentials.[285] The approach potential can influence the breakdown behavior measured using SECCM and may present erroneous results. In addition, there is the possibility of physical contact of the pipette with the substrate. It was shown that by using lower overpotentials (i.e., near the metal's corrosion potential) the pipette physically penetrated the passive film layer to reach the underlying active metal to achieve a current response (Figures 16c, e, and f).[285]

To study insulating passive films without compromising the surface with the pipette, dual-channel pipettes can be utilized (Figure 16b).[286] The feedback signal stems from the potential bias applied between two quasi-reference counter electrodes in each channel that generates an ion conductance current across the liquid meniscus at the pipette tip. The probe signal is then oscillated with a lock-in amplifier to modulate the pipette position

Review
doi.org/10.1002/elsa.202300014
Chemistry Europe
European Chemical Societies Publishing

(distance-modulation) or applied bias (bias-modulation).[287] When the meniscus contacts the substrate, the AC signals (amplitude or phase) are modulated due to the reversible deformation of the droplet, and the pipette is halted before contacting the surface. The dual-channel pipette eliminates the need to apply high overpotentials to the substrate using the single-channel feedback method and hence the probability of the pipette puncturing the passive film. This method was successfully carried out on low-carbon steel in a natural solution (although not an insulating passive film), where no sign of pipette contact was observed (Figure 16d).[54] It is expected that future studies investigating insulating passive films on metals will utilize dual-channel pipettes to avoid experimental artifacts created when using the single-channel method.

4.7 | Advancing knowledge of aging and novel passive metals/coating systems using SEPM

Much of the work reviewed has been performed on freshly prepared passivated metals. Yet, recent research has shown that aging effects on passive films can change their corrosion resistance.[288–290] Aging involves various transformations including film growth, dissolution, recrystallization, defect depletion, stoichiometric changes, and hydration/dehydration of the film.[97] In turn, ionic and electronic conductivity properties will evolve with time. It has been shown that aging may provide improvement to the long-term stability of the passive film and prolong the film's corrosion resistance properties. SEPM studies on aging passive films would enable local, in-situ investigations of film evolution during aging in true, in-service scenarios.

The SEPM methods covered in this review also hold great potential for exploring passivating alloys that have been fabricated using new manufacturing processes. High-entropy alloys (HEAs) have received a great deal of attention in recent years because of their improved physical and chemical properties due to the unique high configurational entropy of these single-phase materials.[291–293] The effect of passivating elements in HEAs could be locally probed using SEPM to gain insight into their effect on passive film properties. Other advanced alloy production methods such as additive manufacturing and metallic thermal spray coatings that undergo passivation could be locally probed for their breakdown susceptibility.[231,294–296]

As highlighted in the recent SECM review on coatings for corrosion protection,[56] SEPM techniques could be of significant importance for understanding the local breakdown of advanced metal coating systems in future research.[27] For instance, a study of the local breakdown sites on modified nitinol surfaces was carried out using feedback and SG/TC modes of SECM.[145] The electrodeposition of tantalum followed by grafting 1-dodecylphsphonic acid self-assembled monolayers resulted in the decrease of the first-order heterogeneous kinetics rate constant of the redox mediator, indicating a reduction of precursor corrosion sites. However, the surface treatment did not eliminate defects completely as revealed by SECM. Another example is the use of SECCM for the local detection of defect-facilitated transport mechanisms for ion-selective membranes.[297] This study demonstrates the applicability of SECCM to diagnose failure mechanisms of corrosion protection coatings, including passive films. SECCM was recently used to screen the structure dependence of a corrosion inhibitor's efficiency on Cu to propose a better inhibitor design.[261] The use of SEPM to locally probe electronic and ionic properties, breakdown susceptibility, and heterogeneity of inhibition strategies such as rare-earth-based coatings,[298–302] lithium-containing coatings,[303,304] phosphate coatings,[305,306] ionic liquid-based coating strategies,[24,307] and organic-based coatings[308,309] are exciting opportunities for future research efforts.

4.8 | Strengthening the connection between SEPM and passive film models

Although there has been much modelling work done to describe passive film growth and breakdown, the mechanisms that lead to compromising passive films are not fully understood. This could be, in part, due to the disconnect between SEPM studies that probe the local electrochemical properties of passive films and the modelling efforts to date.[1] For instance, the point defect model (PDM) developed by Macdonald and coworkers proposed that cation vacancy condensation at the metal-passive film interface is responsible for passivity breakdown.[187,310] The PDM provides analytical expressions for critical breakdown parameters (critical voltage, V_c, and induction time, t_{ind}) independent of film thickness electric field strength. The possible detection of vacancy condensation and/or local film detachment should be explored using SEPM. The high-field model considers that the entire potential drop within a passive film is dependent on film thickness.[311] Systematic studies of thickness, porosity, permeability, and conductivity would provide insight into these passive film models by validating their outcomes and providing localized experimental evidence to the mathematical predictions. By understanding these mechanisms, efficient and long-term protection of metals against corrosion can be better predicted and proposed.

5 | SUMMARY AND FINAL REMARKS

In general, the definition of a passive film remains ambiguous and is often used to describe any decrease in anodic oxidation. This review describes the research efforts within the SEPM community to investigate passivating metals quantitatively. Specifically, SECM, SECCM, and localized electrochemical impedance techniques have provided insight into local passive film variability in microstructural features, film thickness, conductivity, and possibly permeability for different passivating metals and alloys. The effect of redox mediator reactivity on a corroding substrate has been highlighted throughout the discussions as a precaution to take when carrying out SECM in feedback mode to probe the passivation of metals. Yet, the occurrence of oxidative etching may be an indication that a metal is not in a passive state. If oxidative etching does not occur and the metal is under passivated conditions, SECM can be useful for detecting local defects along the passivated surface. It is crucial that correlative microscopy methods are used to discover the true nature of the defects before and after SEPM methods have been used. It is predicted that correlative microscopy methods with SECCM studies will become dominating to probe local passive film properties and breakdown mechanisms. Future developments of SECM and SECCM have been mentioned, including their potential capabilities for extracting quantitative passive film parameters and repassivation kinetics. Locally probing passive film properties in situ may provide insight for passive film models in the future, enabling more quantitative weight to the term "passive."

CONFLICT OF INTEREST STATEMENT

The authors declare no conflicts of interest.

DATA AVAILABILITY STATEMENT

Not applicable.

ORCID

Samantha Michelle Gateman https://orcid.org/0000-0002-3889-9926

REFERENCES

1. D. D. Macdonald, *Pure Appl. Chem.* **1999**, *71*, 951.
2. R. Liu, Z. Zheng, J. Spurgeon, X. Yang, *Energy Environ. Sci.* **2014**, *7*, 2504.
3. J. Shi, X. Zhao, C. Li, *Catalysts* **2023**, *13*, 217.
4. Y. Yang, X. Ning, H. Tang, L. Guo, H. Liu, *Appl. Surf. Sci.* **2014**, *320*, 274.
5. S. Koch, M. Mogensen, P. V. Hendriksen, N. Dekker, B. Rietveld, *Fuel Cells* **2006**, *6*, 117.
6. P. Schwager, D. Fenske, G. Wittstock, *J. Electroanal. Chem.* **2015**, *740*, 82.
7. A. E.-R. El-Sayed, H. A. E.-S. Shilkamy, M. Elrouby, *Sci. Rep.* **2022**, *12*, 18925.
8. V. Maurice, P. Marcus, *Electrochim. Acta* **2012**, *84*, 129.
9. C. F. Schönbein, *Ann. Phys.* **1836**, *113*, 390.
10. V. Maurice, P. Marcus, *Curr. Opin. Solid State Mater. Sci.* **2018**, *22*, 156.
11. The Association for Materials Protection and Performance. (**2021**) *The Association for Materials Protection and Performance's 2021 Impact Canada Study*. https://www.ampp.org/technical-research/what-is-corrosion/corrosion-reference-library/impact-canada
12. H. H. Uhlig, *Corros. Sci.* **1979**, *19*, 777.
13. L. I. Stephens, S. C. Perry, S. M. Gateman, R. Lacasse, R. Schulz, J. Mauzeroll, *J. Electrochem. Soc.* **2017**, *164*, E3576.
14. H.-H. Strehblow, *Electrochim. Acta* **2016**, *212*, 630.
15. E. Sikora, D. D. Macdonald, *Electrochim. Acta* **2002**, *48*, 69.
16. B. Stypula, J. Stoch, *Corros. Sci.* **1994**, *36*, 2159.
17. H. C. Gatos, H. H. Uhlig, *J. Electrochem. Soc.* **1952**, *99*, 250.
18. H. Cong, H. T. Michels, J. R. Scully, *J. Electrochem. Soc.* **2009**, *156*, C16.
19. J. O'. M. Bockris, L. J. V. Minevski, *J. Electroanal. Chem.* **1993**, *349*, 375.
20. N. D. Tomashov, R. M. Altovsky, G. P. Chernova, *J. Electrochem. Soc.* **1961**, *108*, 113.
21. R. E. Meyer, *J. Electrochem. Soc.* **1960**, *107*, 847.
22. D. E. Williams, R. C. Newman, Q. Song, R. G. Kelly, *Nature* **1991**, *350*, 216.
23. A. R. Brooks, C. R. Clayton, K. Doss, Y. C. Lu, *J. Electrochem. Soc.* **1986**, *133*, 2459.
24. A. Z. Benbouzid, O. Gharbi, N. Sidi-Yakoub, M. T. T. Tran, M. Turmine, V. Vivier, *Corros. Commun.* **2023**, *9*, 57. https://doi.org/10.1016/j.corcom.2022.11.001
25. P. B. Raja, M. Ismail, S. Ghoreishiamiri, J. Mirza, M. C. Ismail, S. Kakooei, A. A. Rahim, *Chem. Eng. Commun.* **2016**, *203*, 1145.
26. H. Xiao, Y. Wang, L. Gu, Z. Feng, B. Lei, L. Zhu, H. Guo, G. Meng, *Prog. Org. Coatings* **2023**, *177*, 107418.
27. M. F. Montemor, *Surf. Coatings Technol.* **2014**, *258*, 17.
28. D. E. Tallman, *J. Am. Chem. Soc.* **2004**, *126*, 979.
29. A. A. Darwish, J. Christudasjustus, C. S. Witharamage, R. K. Gupta, *ECS Meet. Abstr.* **2022**, *MA2022-01*, 1005.
30. E. Hamada, K. Yamada, M. Nagoshi, N. Makiishi, K. Sato, T. Ishii, K. Fukuda, S. Ishikawa, T. Ujiro, *Corros. Sci.* **2010**, *52*, 3851.
31. M. Murayama, N. Makiishi, Y. Yazawa, T. Yokota, K. Tsuzaki, *Corros. Sci.* **2006**, *48*, 1307.
32. V. Maurice, W. P. Yang, P. Marcus, *J. Electrochem. Soc.* **1996**, *143*, 1182.
33. D. R. Baer, D. A. Petersen, L. R. Pederson, M. T. Thomas, *J. Vac. Sci. Technol.* **1982**, *20*, 957.
34. H.-H. Strehblow, *J. Electrochem. Soc.* **2021**, *168*, 021510.
35. H.-H. Strehblow, C. M. Melliar-Smith, W. M. Augustyniak, *J. Electrochem. Soc.* **1978**, *125*, 915.
36. M. Brocklebank, J. J. Noël, L. V. Goncharova, *J. Electrochem. Soc.* **2019**, *166*, C3290.
37. D. D. Macdonald, *J. Nucl. Mater.* **2008**, *379*, 24.
38. M. Benoit, C. Bataillon, B. Gwinner, F. Miserque, M. E. Orazem, C. M. Sánchez-Sánchez, B. Tribollet, V. Vivier, *Electrochim. Acta* **2016**, *201*, 340.

39. G. S. Frankel, in *Fundamentals of Corrosion Kinetics* (Eds: A. E. Hughes, J. M. C. Mol, M. L. Zheludkevich, R. G. Buchheit), Springer, Netherlands **2016**, 17–32. https://doi.org/10.1007/978-94-017-7540-3_2
40. P. Marcus, V. Maurice, H.-H. Strehblow, *Corros. Sci.* **2008**, *50*, 2698.
41. G. S. Frankel, *J. Electrochem. Soc.* **1998**, *145*, 2186.
42. J. Soltis, *Corros. Sci.* **2015**, *90*, 5.
43. H. Parangusan, J. Bhadra, N. Al-Thani, *Emergent Mater* **2021**, *4*, 1187.
44. H. Chen, Z. Qin, M. He, Y. Liu, Z. Wu, *Materials* **2020**, *13*, 668.
45. Y. Wang, S. A. Skaanvik, X. Xiong, S. Wang, M. Dong, *Matter* **2021**, *4*, 3483.
46. A. A. Gewirth, B. K. Niece, *Chem. Rev.* **1997**, *97*, 1129.
47. N. Jadhav, V. J. Gelling, *J. Electrochem. Soc.* **2019**, *166*, C3461.
48. A. C. Bastos, M. C. Quevedo, O. V. Karavai, M. G. S. Ferreira, *J. Electrochem. Soc.* **2017**, *164*, C973.
49. B. Łosiewicz, M. Popczyk, A. Smołka, M. Szklarska, P. Osak, A. Budniok, *Solid State Phenom.* **2015**, *228*, 383–393.
50. B. Ballesteros Katemann, *Electrochem. Commun.* **2002**, *4*, 134.
51. C. Örnek, C. Leygraf, J. Pan, *Corros. Eng. Sci. Technol.* **2019**, *54*, 185.
52. N. A. Payne, L. I. Stephens, J. Mauzeroll, *Corrosion* **2017**, *73*, 759–780.
53. T. Suter, H. Böhni, *Electrochim. Acta* **1997**, *42*, 3275.
54. L. C. Yule, C. L. Bentley, G. West, B. A. Shollock, P. R. Unwin, *Electrochim. Acta* **2019**, *298*, 80.
55. H. Luo, C. Dong, S. Gao, C. Du, K. Xiao, X. Li, *RSC Adv.* **2014**, *4*, 56582.
56. J. J. Santana, J. Izquierdo, R. M. Souto, *Coatings* **2022**, *12*, 637.
57. I. Traxler, T. D. Singewald, G. Schimo-Aichhorn, S. Hild, M. Valtiner, *Corros. Rev.* **2022**, *40*, 515.
58. D. Polcari, P. Dauphin-Ducharme, J. Mauzeroll, *Chem. Rev.* **2016**, *116*, 13234.
59. S. M. Gateman, L. I. Stephens, S. C. Perry, R. Lacasse, R. Schulz, J. Mauzeroll, *npj Mater. Degrad.* **2018**, *2*, 5.
60. D. O. Wipf, *Eng. Asp.* **1994**, *93*, 251.
61. A. Estrada-Vargas, A. Bandarenka, V. Kuznetsov W. Schuhmann, *Anal. Chem.* **2016**, *88*, 3354.
62. J. Kwak, A. J. Bard, *Anal. Chem.* **1989**, *61*, 1221.
63. C. Lefrou, R. Cornut, *Chem. Phys. Chem* **2010**, *11*, 547.
64. S. Kuss, D. Polcari, M. Geissler, D. Brassard, J. Mauzeroll, *Proc. Natl. Acad. Sci. USA* **2013**, *110*, 9249.
65. S. A. Skaanvik, L. I. Stephens, S. M. Gateman, M. Geissler, J. Mauzeroll, *Anal. Chem.* **2022**, *94*, 13852.
66. N. Leslie, E. Mena-Morcillo, A. Morel, J. Mauzeroll, *Anal. Chem.* **2022**, *94*, 15315.
67. F. Zhou, P. R. Unwin, A. J. Bard, *J. Phys. Chem.* **1992**, *96*, 4917.
68. Y. Yin, L. Niu, M. Lu, W. Guo, S. Chen, *Appl. Surf. Sci.* **2009**, *255*, 9193.
69. A. Asserghine, M. Medvidovic-Kosanovic, A. Stankovic, L. Nagy, R. M. Souto, G. Nagy, *Sensors Actuators B Chem.* **2020**, *321*, 128610.
70. Q. Zhang, P. Liu, Z. Zhu, J. Zhang, F. Cao, *Corros. Sci.* **2020**, *164*, 108312.
71. A. S. Bandarenka, A. Maljusch, V. Kuznetsov, K. Eckhard, W. Schuhmann, *J. Phys. Chem. C* **2014**, *118*, 8952.
72. O. Gharbi, K. Ngo, M. Turmine, V. Vivier, *Curr. Opin. Electrochem.* **2020**, *20*, 1.
73. M. Pereira Gomes, S. Michelle Gateman, I. Costa, O. Gharbi, K. Ngo, J. Luiz Rossi, M. Turmine, V. Vivier, *Measurement* **2022**, *200*, 111504.
74. V. Shkirskiy, P. Volovitch, V. Vivier, *Electrochim. Acta* **2017**, *235*, 442.
75. C. Gabrielli, F. Huet, M. Keddam, P. Rousseau, V. Vivier, *J. Phys. Chem. B* **2004**, *108*, 11620.
76. A. S. Baranski, A. Szulborska, *Electrochim. Acta* **1996**, *41*, 985.
77. K. Eckhard, M. Etienne, A. Schulte, W. Schuhmann, *Electrochem. Commun.* **2007**, *9*, 1793.
78. H. Böhni, T. Suter, A. Schreyer, *Electrochim. Acta* **1995**, *40*, 1361.
79. T. Suter, H. Böhni, *Electrochim. Acta* **1998**, *43*, 2843.
80. C. L. Bentley, J. Edmondson, G. N. Meloni, D. Perry, V. Shkirskiy, P. R. Unwin, *Anal. Chem.* **2019**, *91*, 84.
81. C. L. Bentley, M. Kang, P. R. Unwin, *Curr. Opin. Electrochem.* **2017**, *6*, 23.
82. L. Cheng, R. Jin, D. Jiang, J. Zhuang, X. Liao, Q. Zheng, *Anal. Chem.* **2021**, *93*, 16401.
83. V. Shkirskiy, L. C. Yule, E. Daviddi, C. L. Bentley, J. Aarons, G. West, P. R. Unwin, *J. Electrochem. Soc.* **2020**, *167*, 041507.
84. S. M. Gateman, O. Gharbi, M. Turmine, V. Vivier, *Electrochim. Acta* **2021**, *399*, 139402.
85. M. M. Lohrengel, A. Moehring, M. Pilaski, *Electrochim. Acta* **2001**, *47*, 137.
86. L. C. Yule, V. Shkirskiy, J. Aarons, G. West, B. A. Shollock, C. L. Bentley, P. R. Unwin, *Electrochim. Acta* **2020**, *332*, 135267.
87. S. M. Gateman, N. S. Georgescu, M.-K. Kim, I.n-H.o Jung, J. Mauzeroll, *J. Electrochem. Soc.* **2019**, *166*, C624.
88. Y. Li, A. Morel, D. Gallant, J. Mauzeroll, *Anal. Chem.* **2020**, *92*, 12415.
89. X. Xu, D. Valavanis, P. Ciocci, S. Confederat, F. Marcuccio, J.-F. Lemineur, P. Actis, F. Kanoufi, P. R. Unwin, *Anal. Chem.* **2023**, *95*, 319.
90. L. Danis, D. Polcari, A. Kwan, S. M. Gateman, J. Mauzeroll, *Anal. Chem.* **2015**, *87*, 2565.
91. R. S. Lillard, P. J. Moran, H. S. Isaacs, *J. Electrochem. Soc.* **1992**, *139*, 1007.
92. P. Martínez-Viademonte, S. Abrahami, T. Hack, M. Burchardt, H. Terryn, *Coatings* **2020**, *10*, 1106.
93. T. Ma, G.-L. Xu, Y. Li, L. Wang, X. He, J. Zheng, J. Liu, M. H. Engelhard, P. Zapol, L. A. Curtiss, J. Jorne, K. Amine, Z. Chen, *J. Phys. Chem. Lett.* **2017**, *8*, 1072.
94. B. K. Park, Y. K. Jeong, S.o Y. Yang, S. Kwon, J. H. Yang, Y. M. Kim, K. J. Kim, *J. Power Sources* **2021**, *506*, 230222.
95. H.u Zhou, D. Chhin, A. Morel, D. Gallant, J. Mauzeroll, *npj Mater. Degrad.* **2022**, *6*, 20.
96. I. Serebrennikova, H. S. White, *Electrochem. Solid-State Lett.* **2001**, *4*, B4.
97. J. W. Schultze, M. M. Lohrengel, *Electrochim. Acta* **2000**, *45*, 2499.
98. G. E. Thompson, G. C. Wood, *Treatise Mater. Sci. Technol.* **1983**, *23*, 205.
99. I. Serebrennikova, S. Lee, H. S. White, *Faraday Discuss.* **2002**, *121*, 199.
100. M. B. Jensen, A. Guerard, D. E. Tallman, G. P. Bierwagen, *J. Electrochem. Soc.* **2008**, *155*, C324.

101. S. Gialanella, A. Malandruccolo, in *Alloys for Aircraft Structures BT - Aerospace Alloys* (Eds: S. Gialanella, A. Malandruccolo), Springer International Publishing **2020**, 41–127. https://doi.org/10.1007/978-3-030-24440-8_3
102. A. E. Hughes, N. Birbilis, J. M. C. Mol, S. J. Garcia, X. Zhou, G. E. Thompson, *Degrad. Alum. Alloy.* **2011**, *1*, 223.
103. J. C. Seegmiller, D. A. Buttry, *J. Electrochem. Soc.* **2003**, *150*, B413.
104. C. He, W. Mo, Y. Zheng, S. P. Feng, B. Luo, *J. Alloys Compd.* **2021**, *888*, 161596.
105. L. Di?Az-Ballote, L. Veleva, M. A. Pech-Canul, M. I. Pech-Canul, D. O. Wipf?, *J. Electrochem. Soc.* **2004**, *151*, B299.
106. A. Davoodi, J. Pan, C. Leygraf, S. Norgren, *J. Electrochem. Soc.* **2008**, *155*, C211.
107. A. Davoodi, J. Pan, C. Leygraf, S. Norgren, *Electrochem. Solid-State Lett.* **2005**, *8*, B21.
108. A. Davoodi, J. Pan, C. Leygraf, S. Norgren, *Electrochim. Acta* **2007**, *52*, 7697.
109. A. Davoodi, J. Pan, C. Leygraf, S. Norgren, *Appl. Surf. Sci.* **2006**, *252*, 5499.
110. H. Krawiec, Z. Szklarz, *Electrochim. Acta* **2016**, *203*, 426.
111. H. Krawiec, V. Vignal, Z. Szklarz, *J. Solid State Electrochem.* **2008**, *13*, 1181.
112. Y. Li, A. Morel, D. Gallant, J. Mauzeroll, *ACS Appl. Mater. Interfaces* **2022**, *14*, 47230.
113. J. Schöchlin, K. P. Bohnen, K. M. Ho, *Surf. Sci.* **1995**, *324*, 113.
114. M. I. Baskes, *Phys. Rev. B* **1992**, *46*, 2727.
115. M. Li, Y. Wang, B. Blount, E. Gordon, J. A. Muñoz-Castañeda, Z. Ye, H. Ren, *Nano Lett.* **2022**, *22*, 6313.
116. C. Corvalán Moya, M. J. Iribarren, N. Di Lalla, F. Dyment, *J. Nucl. Mater.* **2008**, *382*, 35.
117. B. A. Cheadle, *The Physical Metallurgy of Zirconium Alloys*. Atomic Energy of Canada Limited **1975**.
118. P. Meisterjahn, H. W. Hoppe, J. W. Schultze, *J. Electroanal. Chem. Interfacial Electrochem.* **1987**, *217*, 159.
119. F. Hua, K. Mon, P. Pasupathi, G. Gordon, D. Shoesmith, *Corrosion* **2005**, *61*, 987–1003.
120. A. Merati, B. Cox, *Corrosion* **1999**, *55*, 388.
121. P. Rudling, G. Wikmark, *J. Nucl. Mater.* **1999**, *265*, 44.
122. C. Degueldre, J. Raabe, G. Kuri, S. Abolhassani, *Talanta* **2008**, *75*, 402.
123. A. R. Massih, T. Andersson, P. Witt, M. Dahlbäck, M. Limbäck, *J. Nucl. Mater.* **2003**, *322*, 138.
124. J. A. Sawicki, *J. Nucl. Mater.* **1996**, *228*, 238.
125. C. Nowierski, J. J. Noël, D. W. Shoesmith, Z. Ding, *Electrochem. Commun.* **2009**, *11*, 1234.
126. C. Nowierski, J. J. Noël, D. W. Shoesmith, Z. Ding, *J. Electrochem. Soc.* **2012**, *159*, C590.
127. F. Song, M. M. Busch, B. Lassalle-Kaiser, C.-S. Hsu, E. Petkucheva, M. Bensimon, H. M. Chen, C. Corminboeuf, X. Hu, *ACS Cent. Sci.* **2019**, *5*, 558.
128. M. Gong, D.i-Y. Wang, C.-C. Chen, B.-J. Hwang, H. Dai, *Nano Res.* **2016**, *9*, 28.
129. T. He, Q. Liu, H. Fan, Y. Yang, H. Wang, S. Zhang, R. Che, E. Wang, *Int. J. Hydrogen Energy* **2023**, *48*, 19385.
130. P. Hajjar, M.-A. Lacour, N. Masquelez, J. Cambedouzou, S. Tingry, D. Cornu, Y. Holade, *Molecules* **2021**, *26*, 5926.
131. L. Wang, J. Wang, L. Wang, M. Zhang, R. Wang, C. Zhan, *Int. J. Miner. Metall. Mater.* **2022**, *29*, 925.
132. Z. Zeng, W. Zhao, S. Yuan, Y.u Dong, J. Zhu, F. Jiang, Y. Yang, S. Liu, L.i Wang, P. Ge, *ACS Appl. Energy Mater.* **2022**, *5*, 9189.
133. H. S. Klapper, N. S. Zadorozne, R. B. Rebak, *Acta Metall. Sin. (English Lett.)* **2017**, *30*, 296.
134. R. M. Carranza, M. A. Rodríguez, *npj Mater. Degrad.* **2017**, *1*, 9.
135. C. H. Paik, R. C. Alkire, *J. Electrochem. Soc.* **2001**, *148*, B276.
136. L. Verchère, I. Aubert, O. Devos, *Electrochim. Acta* **2019**, *313*, 292.
137. C. A. Schuh, K. Anderson, C. Orme, *Surf. Sci.* **2003**, *544*, 183.
138. T. Duerig, A. Pelton, D. Stöckel, *Mater. Sci. Eng. A* **1999**, *273–275*, 149.
139. N. B. Morgan, *Mater. Sci. Eng. A* **2004**, *378*, 16.
140. D. J. Wever, A. G. Veldhuizen, J. De Vries, H. J. Busscher, D. R. A. Uges, J. R. Van Horn, *Biomaterials* **1998**, *19*, 761.
141. I. Milosev, B. Kapun, *Mater. Sci. Eng. C* **2012**, *32*, 1087.
142. M. Es-Souni, M. Es-Souni, H. Fischer-Brandies, *Anal. Bioanal. Chem.* **2005**, *381*, 557.
143. A. Schulte, S. Belger, M. Etienne, W. Schuhmann, *Mater. Sci. Eng. A* **2004**, *378*, 523.
144. J. Izquierdo, M. B. González-Marrero, M. Bozorg, B. M. Fernández-Pérez, H. C. Vasconcelos, J. J. Santana, R. M. Souto, *Electrochim. Acta* **2016**, *203*, 366.
145. A. Maho, F. Kanoufi, C. Combellas, J. Delhalle, Z. Mekhalif, *Electrochim. Acta* **2014**, *116*, 78.
146. D. Ruhlig, H. Gugel, A. Schulte, W. Theisen, W. Schuhmann, *Analyst* **2008**, *133*, 1700.
147. A. Asserghine, M. Medvidovic-Kosanovic, L. Nagy, G. Nagy, *Electrochem. Commun.* **2019**, *107*, 106539.
148. M. C. Pereira, M. L. Pereira, J. P. Sousa, *J. Biomed. Mater. Res.* **1998**, *40*, 40.
149. P. H. Gitlitz, F. W. Sunderman, P. J. Goldblatt, *Toxicol. Appl. Pharmacol.* **1975**, *34*, 430.
150. N. Mazinanian, Y. Hedberg, *Regul. Toxicol. Pharmacol.* **2013**, *65*, 135.
151. M. Kaur, K. Singh, *Mater. Sci. Eng. C* **2019**, *102*, 844.
152. M. Manßen, L. L. Schafer, *Chem. Soc. Rev.* **2020**, *49*, 6947.
153. Q. Zhao, Q. Sun, S. Xin, Y. Chen, C. Wu, H. Wang, J. Xu, M. Wan, W. Zeng, Y. Zhao, *Mater. Sci. Eng. A* **2022**, *845*, 143260.
154. J. Pan, D. Thierry, C. Leygraf, *Electrochim. Acta* **1996**, *41*, 1143.
155. S. L. D.e Assis, S. Wolynec, I. Costa, *Electrochim. Acta* **2006**, *51*, 1815.
156. J. R. Birch, T. D. Burleigh, *Corrosion* **2000**, *56*, 1233.
157. A. M. Schmidt, D. S. Azambuja, E. M. A. Martini, *Corros. Sci.* **2006**, *48*, 2901.
158. Y. Z. Huang, D. J. Blackwood, *Electrochim. Acta* **2005**, *51*, 1099.
159. B. Roh, D. D. Macdonald, *Russ. J. Electrochem.* **2007**, *43*, 125.
160. D.e-S. Kong, W.-H. Lu, Y.-Y. Feng, Z.-Y.u Yu, J.i-X. Wu, W.-J. Fan, H.-Y. Liu, *J. Electrochem. Soc.* **2009**, *156*, C39.
161. E. N. Paleolog, A. Z. Fedotova, O. G. Derjagina, N. D. Tomashov, *J. Electrochem. Soc.* **1978**, *125*, 1410.
162. I. Dugdale, J. B. Cotton, *Corros. Sci.* **1964**, *4*, 397.
163. D. Sazou, K. Saltidou, M. Pagitsas, *Electrochim. Acta* **2012**, *76*, 48.
164. T. R. Beck, *J. Electrochem. Soc.* **1973**, *120*, 1310.
165. T. R. Beck, *J. Electrochem. Soc.* **1973**, *120*, 1317.
166. S. Huo, X. Meng, *Corros. Sci.* **1990**, *31*, 281.
167. N. Casillas, S. J. Charlebois, W. H. Smyrl, H. S. White, *J. Electrochem. Soc.* **1993**, *140*, L142.

168. N. Casillas, S. R. Snyder, W. H. Smyrl, H. S. White, *J. Phys. Chem.* **1991**, *95*, 7002.
169. C. J. Boxley, H. S. White, C. E. Gardner, J. V. Macpherson, *J. Phys. Chem. B* **2003**, *107*, 9677.
170. N. Casillas, S. Charlebois, W. H. Smyrl, H. S. White, *J. Electrochem. Soc.* **1994**, *141*, 636.
171. K. Fushimi, T. Okawa, M. Seo, *Electrochemistry* **2000**, *68*, 950.
172. S. B. Basame, H. S. White, *J. Phys. Chem. B* **1998**, *102*, 9812.
173. S. B. Basame, H. S. White, *J. Phys. Chem.* **1995**, *99*, 16430.
174. A. Asserghine, M. Medvidovic-Kosanovic, L. Nagy, R. M. Souto, G. Nagy, *Sensors Actuators B Chem* **2020**, *320*, 128339.
175. X.-R. Li, Q.-H. Zhang, X.-Z. Meng, L.-K. Wu, F.-H. Cao, *Corros. Sci.* **2021**, *191*, 109726.
176. I. Chattoraj in *10 – Stress Corrosion Cracking (SCC) and Hydrogen-Assisted Cracking in Titanium Alloys* (Eds: V. S. Raja, T. B. Shoji T.-S. C. C.), Woodhead Publishing **2011**, 381–408. https://doi.org/10.1533/9780857093769.3.381
177. R. Zhu, C. Nowierski, Z. Ding, J. J. Noël, D. W. Shoesmith, *Chem. Mater.* **2007**, *19*, 2533.
178. R. Zhu, Z. Qin, J. J. Noël, D. W. Shoesmith, Z. Ding, *Anal. Chem.* **2008**, *80*, 1437.
179. S. E. Pust, D. Scharnweber, S. Baunack, G. Wittstock, *J. Electrochem. Soc.* **2007**, *154*, C508.
180. D.-I. Seo, J.-B. Lee, *J. Electrochem. Soc.* **2019**, *166*, C428.
181. M. Iannuzzi, G. S. Frankel, *npj Mater. Degrad.* **2022**, *6*, 101.
182. M. Pourbaix, *Atlas of Electrochemical Equilibria in Aqueous Solutions*, Pergamon Press **1966**. https://mcgill.on.worldcat.org/oclc/2168509
183. I. V. Sieber, H. Hildebrand, S. Virtanen, P. Schmuki, *Corros. Sci.* **2006**, *48*, 3472.
184. M.-I. Nagayama, M. Cohen, *J. Electrochem. Soc.* **1962**, *109*, 781.
185. A. J. Davenport, L. J. Oblonsky, M. P. Ryan, M. F. Toney, *J. Electrochem. Soc.* **2000**, *147*, 2162.
186. R. M. Cornell, U. Schwertmann *The Iron Oxides: Structure, Properties, Reactions, Occurrences, and Uses*, Vol. *664*, Wiley-vch Weinheim **2003**.
187. D. D. Macdonald, *J. Electrochem. Soc.* **1992**, *139*, 3434.
188. S. C. Perry, S. M. Gateman, L. I. Stephens, R. Lacasse, R. Schulz, J. Mauzeroll, *J. Electrochem. Soc.* **2019**, *166*, C3186.
189. R. P. Frankenthal, *Electrochim. Acta* **1971**, *16*, 1845.
190. K. J. Vetter, F. Gorn, *Electrochim. Acta* **1973**, *18*, 321.
191. T. R. Beck, *J. Electrochem. Soc.* **1982**, *129*, 2412.
192. B. Mazurkiewicz, *Electrochim. Acta* **1993**, *38*, 495.
193. K. Fushimi, Y. Takabatake, T. Nakanishi, Y. Hasegawa, *Electrochim. Acta* **2013**, *113*, 741.
194. K. Fushimi, K. Azumi, M. Seo, *ISIJ Int.* **1999**, *39*, 346.
195. K. Fushimi, M. Seo, *Electrochim. Acta* **2001**, *47*, 121.
196. A. Schreiber, J. W. Schultze, M. M. Lohrengel, F. Kármán, E. Kálmán, *Electrochim. Acta* **2006**, *51*, 2625.
197. Y. Takabatake, K. Fushimi, T. Nakanishi, Y. Hasegawa, *J. Electrochem. Soc.* **2014**, *161*, C594.
198. J. Izquierdo, A. Eifert, C. Kranz, R. M. Souto, *ChemElectroChem* **2015**, *2*, 1847.
199. J. W. Still, D. O. Wipf, *J. Electrochem. Soc.* **1997**, *144*, 2657.
200. J. Izquierdo, A. Eifert, R. M. Souto, C. Kranz, *Electrochem. Commun.* **2015**, *51*, 15.
201. D. Dwivedi, K. Lepková, T. Becker, *RSC Adv.* **2017**, *7*, 4580.
202. K. Fushimi, K. Yanagisawa, T. Nakanishi, Y. Hasegawa, T. Kawano, M. Kimura, *Electrochim. Acta* **2013**, *114*, 83.
203. K. A. Lill, K. Fushimi, M. Seo, A. W. Hassel, *J. Appl. Electrochem.* **2008**, *38*, 1339.
204. K. A. Lill, A. W. Hassel, G. Frommeyer, M. Stratmann, *Electrochim. Acta* **2005**, *51*, 978.
205. L. C. Yule, V. Shkirskiy, J. Aarons, G. West, C. L. Bentley, B. A. Shollock, P. R. Unwin, *J. Phys. Chem. C* **2019**, *123*, 24146.
206. K. Yanagisawa, T. Nakanishi, Y. Hasegawa, K. Fushimi, *J. Electrochem. Soc.* **2015**, *162*, C322.
207. J. Jun, K. Holguin, G. S. Frankel, *Corrosion* **2014**, *70*, 146–155.
208. A. Pardo, M. C. Merino, A. E. Coy, F. Viejo, R. Arrabal, E. Matykina, *Corros. Sci.* **2008**, *50*, 1796.
209. J. Ma, B. Zhang, J. Wang, G. Wang, E.-H. Han, W. Ke, *Corros. Sci.* **2010**, *52*, 2867.
210. D. E. Williams, T. F. Mohiuddin, Y. Y. Zhu, *J. Electrochem. Soc.* **1998**, *145*, 2664.
211. T. E. Lister, P. J. Pinhero, *Electrochim. Acta* **2003**, *48*, 2371.
212. C. H. Paik, H. S. White, R. C. Alkire, *J. Electrochem. Soc.* **2000**, *147*, 4120.
213. S. G. Acharyya, A. Khandelwal, V. Kain, A. Kumar, I. Samajdar, *Mater. Charact.* **2012**, *72*, 68.
214. Y. Xia, F. Cao, W. Liu, L. Chang, J. Zhang, *Int. J. Electrochem. Sci.* **2013**, *8*, 3057.
215. N. R. Baddoo, *J. Constr. Steel Res.* **2008**, *64*, 1199.
216. M. Cortie, M. S. du Toit, F. Steels, *Reference Module in Materials Science and Materials Engineering*, Elsevier **2016**. https://doi.org/10.1016/B978-0-12-803581-8.02501-7
217. G. S. Was, S. Ukai, in *Structural Alloys for Nuclear Energy Applications* (Eds: G. R. Odette, S. J. Zinkle), Elsevier **2019**, 293–347. https://doi.org/10.1016/B978-0-12-397046-6.00008-3
218. Y. Murakami, in *Metal Fatigue* (Ed: Y. B. Murakami), 2nd edition, Elsevier **2019**, 431–451. https://doi.org/10.1016/B978-0-12-813876-2.00017-0
219. A. J. Bard, M. Stratmann, G. S. Frankel, *Encyclopedia of Electrochemistry, Volume 4, Corrosion and Oxide Films*, Wiley-VCH Verlag GmbH **2003**.
220. C. F. Dong, H. Luo, K. Xiao, X. G. Li, Y. F. Cheng, *J. Mater. Eng. Perform.* **2012**, *21*, 406.
221. Y. González-Garci?A, G. T. Burstein, S. González, R. M. Souto, *Electrochem. Commun.* **2004**, *6*, 637.
222. I. Annergren, D. Thierry, F. Zou, *J. Electrochem. Soc.* **1997**, *144*, 1208.
223. I. Annergren, F. Zou, D. Thierry, *Electrochim. Acta* **1999**, *44*, 4383.
224. L. B. Coelho, D. Torres, M. Bernal, G. M. Paldino, G. Bontempi, J. Ustarroz, *Corros. Sci.* **2023**, *217*, 111104.
225. M. P. Ryan, D. E. Williams, R. J. Chater, B. M. Hutton, D. S. Mcphail, *Nature* **2002**, *415*, 770.
226. I. Muto, Y. Izumiyama, N. Hara, *J. Electrochem. Soc.* **2007**, *154*, C439.
227. H. Y. Ha, C. J. Park, H. S. Kwon, *Corros. Sci.* **2007**, *49*, 1266.
228. F. Arjmand, A. Adriaens, *Electrochim. Acta* **2012**, *59*, 222.
229. B. Gwinner, M. Auroy, F. Balbaud-Célérier, P. Fauvet, N. Larabi-Gruet, P. Laghoutaris, R. Robin, *Corros. Sci.* **2016**, *107*, 60.
230. R. Oltra, B. Vuillemin, F. Thebault, F. Rechou, *Electrochem. Commun.* **2008**, *10*, 848.
231. S. M. Gateman, I. Halimi, A. R. Costa Nascimento, R. Lacasse, R. Schulz, C. Moreau, R. Chromik, J. Mauzeroll, *npj Mater. Degrad.* **2019**, *3*, 25.

232. J. Orlikowski, K. Darowicki, A. Arutunow, W. Jurczak, *J. Electroanal. Chem.* **2005**, *576*, 277.
233. R. N. Clark, R. Burrows, R. Patel, S. Moore, K. R. Hallam, P. E. J. Flewitt, *Heliyon* **2020**, *6*, e03448.
234. P. Sun, Z. Liu, H. Yu, M. V. Mirkin, *Langmuir* **2008**, *24*, 9941.
235. D. Sidane, O. Devos, M. Puiggali, M. Touzet, B. Tribollet, V. Vivier, *Electrochem. Commun.* **2011**, *13*, 1361.
236. R. K. Zhu, J. L. Luo, *Electrochem. Commun.* **2010**, *12*, 1752.
237. A. Nazarov, V. Vivier, D. Thierry, F. Vucko, B. Tribollet, *J. Electrochem. Soc.* **2017**, *164*, C66.
238. A. Yazdanpanah, M. Franceschi, R. I. Revilla, S. Khademzadeh, I. De Graeve, M. Dabalà, *Corros. Sci.* **2022**, *208*, 110642.
239. A. Yazdanpanah, L. Pezzato, M. Dabalà, *Eng. Fail. Anal.* **2022**, *142*, 106797.
240. M. Breimesser, S. Ritter, H.-P. Seifert, S. Virtanen, T. Suter, *Corros. Sci.* **2012**, *55*, 126.
241. L. C. Yule, E. Daviddi, G. West, C. L. Bentley, P. R. Unwin, *J. Electroanal. Chem.* **2020**, *872*, 114047.
242. H. Torbati-Sarraf, A. Poursaee, *Materialia* **2018**, *2*, 19.
243. D. S. Hall, M. Behazin, W. Jeffrey Binns, P. G. Keech, *Prog. Mater. Sci.* **2021**, *118*, 100766.
244. F. King, *Corrosion* **2013**, *69*, 986.
245. L. P. Andersen, R. Thakar, A. H. Sulatn, *Clin. Microbiol. Rev.* **2019**, *32*, e00125.
246. I. Salah, I. P. Parkin, E. Allan, *RSC Adv.* **2021**, *11*, 18179.
247. H. Timonen, *Contraception* **1976**, *14*, 25.
248. X. Bilian, *Best Pract. Res. Clin. Obstet. Gynaecol.* **2002**, *16*, 155–168.
249. F. Mao, C. Dong, S. Sharifi-Asl, P. Lu, D. D. Macdonald, *Electrochim. Acta* **2014**, *144*, 391.
250. Z. Qin, R. Daljeet, M. Ai, N. Farhangi, J. J. Noël, S. Ramamurthy, D. Shoesmith, F. King, P. Keech, *Corros. Eng. Sci. Technol.* **2017**, *52*, 45.
251. C. Dong, F. Mao, S. Gao, S. Sharifi-Asl, P. Lu, D. D. Macdonald, *J. Electrochem. Soc.* **2016**, *163*, C707.
252. T. Martino, R. Partovi-Nia, J. Chen, Z. Qin, D. W. Shoesmith, *Electrochim. Acta* **2014**, *127*, 439.
253. M. Guo, J. Chen, C. Lilja, V. Dehnavi, M. Behazin, J. J. Noël, D. W. Shoesmith, *Electrochim. Acta* **2020**, *362*, 137087.
254. J. Chen, Z. Qin, D. W. Shoesmith, *J. Electrochem. Soc.* **2010**, *157*, C338.
255. J. Izquierdo, A. Eifert, C. Kranz, R. M. Souto, *Electrochim. Acta* **2017**, *247*, 588.
256. J. V. Macpherson, C. J. Slevin, P. R. Unwin, *J. Chem. Soc. Faraday Trans.* **1996**, *92*, 3799.
257. D. Mandler, A. J. Bard, *J. Electrochem. Soc.* **1989**, *136*, 3143.
258. D. Ruhlig, W. Schuhmann, *Electroanalysis* **2007**, *19*, 191.
259. E. Martinez-Lombardia, Y. Gonzalez-Garcia, L. Lapeire, I. De Graeve, K. Verbeken, L. Kestens, J. M. C. Mol, H. Terryn, *Electrochim. Acta* **2014**, *116*, 89.
260. O. J. Wahab, M. Kang, E. Daviddi, M. Walker, P. R. Unwin, *ACS Catal.* **2022**, *12*, 6578.
261. E. Daviddi, V. Shkirskiy, P. M. Kirkman, M. P. Robin, C. L. Bentley, P. R. Unwin, *J. Phys. Chem. C* **2022**, *126*, 14897.
262. A. M. Ashmawy, R. Said, I. A. Naguib, B.o Yao, M. A. Bedair, *ACS Omega* **2022**, *7*, 17849.
263. G. Kear, B. D. Barker, F. C. Walsh, *Corros. Sci.* **2004**, *46*, 109.
264. Z. Wang, Y. Li, X. Jiang, C. Pan, *MRS Adv.* **2017**, *2*, 2033.
265. L. Guadagnini, C. Chiavari, C. Martini, E. Bernardi, L. Morselli, D. Tonelli, *Electrochim. Acta* **2011**, *56*, 6598.
266. A. Dobkowska, M. D. H. Castillo, J. P. Turnbull, S. Ramamurthy, D. Zagidulin, D. E. Moser, M. Behazin, P. G. Keech, D. W. Shoesmith, J. J. Noël, *Corros. Sci.* **2021**, *192*, 109778.
267. R. M. Asmussen, W. J. Binns, P. Jakupi, P. Dauphin-Ducharme, U. M. Tefashe, J. Mauzeroll, D. Shoesmith, *Corros. Sci.* **2015**, *93*, 70.
268. P. Dauphin-Ducharme, C. Kuss, D. Rossouw, N. A. Payne, L. Danis, G. A. Botton, J. Mauzeroll, *J. Electrochem. Soc.* **2015**, *162*, C677.
269. O. E. Hüsser, D. H. Craston, A. J. Bard, *J. Electrochem. Soc.* **1989**, *136*, 3222.
270. R. Thakar, R. Zakeri, C. A. Morris, L. A. Baker, *Anal. Methods* **2012**, *4*, 4353.
271. M. Shen, R. Ishimatsu, J. Kim, S. Amemiya, *J. Am. Chem. Soc.* **2012**, *134*, 9856.
272. C. Kuss, N. A. Payne, J. Mauzeroll, *J. Electrochem. Soc.* **2016**, *163*, H3066.
273. S.-Y. Tan, D. Perry, P. R. Unwin, *J. Electroanal. Chem.* **2018**, *819*, 240.
274. S. B. Basame, H. S. White, *Anal. Chem.* **1999**, *71*, 3166.
275. P. K. Hansma, B. Drake, O. Marti, S. A. C. Gould, C. B. Prater, *Science* **1989**, *243*, 641.
276. A. Page, D. Perry, P. R. Unwin, *Proc. R. Soc. A Math. Phys. Eng. Sci.* **2017**, *473*, 20160889.
277. W. J. Paschoalino, N. A. Payne, T. M. Pessanha, S. M. Gateman, L. T. Kubota, J. Mauzeroll, *Anal. Chem.* **2020**, *92*, 10300.
278. S. Møller Sønderskov, L. Hyldgaard Klausen, S. Amland Skaanvik, X. Han, M. Dong, *ChemPhysChem* **2020**, *21*, 1474.
279. Y. Takahashi, A. I. Shevchuk, P. Novak, Y. Murakami, H. Shiku, Y. E. Korchev, T. Matsue, *J. Am. Chem. Soc.* **2010**, *132*, 10118.
280. D. A. Walsh, J. L. Fernández, J. Mauzeroll, A. J. Bard, *Anal. Chem.* **2005**, *77*, 5182.
281. K. Jüttner, *Electrochim. Acta* **1990**, *35*, 1501.
282. V. Vivier, M. E. Orazem, *Chem. Rev.* **2022**, *122*, 11131.
283. C. G. Williams, M. A. Edwards, A. L. Colley, J. V. Macpherson, P. R. Unwin, *Anal. Chem.* **2009**, *81*, 2486.
284. D. Zhan, D. Yang, Y. Zhu, X. Wu, Z.-Q. Tian, *Chem. Commun.* **2012**, *48*, 11449.
285. Y. Li, A. Morel, D. Gallant, J. Mauzeroll, *Anal. Chem.* **2022**, *94*, 14603.
286. N. Ebejer, A. G. Güell, S. C. S. Lai, K. Mckelvey, M. E. Snowden, P. R. Unwin, *Annu. Rev. Anal. Chem.* **2013**, *6*, 329.
287. K. McKelvey, D. Perry, J. C. Byers, A. W. Colburn, P. R. Unwin, *Anal. Chem.* **2014**, *86*, 3639.
288. P. Aldhous, R. Akid, R. Leiva-Garcia, S. Zhou, *Mater. Corros.* **2023**, *74*, 373.
289. G. S. Frankel, T. Li, J. R. Scully, *J. Electrochem. Soc.* **2017**, *164*, C180.
290. J. R. Scully, E. Romanovskaia, K. Lutton, A. Y. Gerard, S. B. Inman, *ECS Meet. Abstr.* **2022**, *733*, MA2022-02,.
291. K. Yamanaka, H. Shiratori, M. Mori, K. Omura, T. Fujieda, K. Kuwabara, A. Chiba, *npj Mater. Degrad.* **2020**, *4*, 24.
292. Y. Qiu, M. A. Gibson, H. L. Fraser, N. Birbilis, *Mater. Sci. Technol.* **2015**, *31*, 1235.
293. Y. Qiu, S. Thomas, M. A. Gibson, H. L. Fraser, N. C. Birbilis, *npj Mater. Degrad.* **2017**, *1*, 15.

294. G. Sander, J. Tan, P. Balan, O. Gharbi, D. R. Feenstra, L. Singer, S. Thomas, R. G. Kelly, J. R. Scully, N. Birbilis, *Corrosion* **2018**, *74*, 1318.
295. S. M. Gateman, K. Page, I. Halimi, A. R. C. Nascimento, S. Savoie, R. Schulz, C. Moreau, I. P. Parkin, J. Mauzeroll, *ACS Appl. Mater. Interfaces* **2020**, *12*, 1523.
296. D. A. Walsh, L. E. Li, M. S. Bakare, K. T. Voisey, *Electrochim. Acta* **2009**, *54*, 4647.
297. C. L. Bentley, M. Kang, S. Bukola, S. E. Creager, P. R. Unwin, *ACS Nano* **2022**, *16*, 5233.
298. D. Bienstock, J. H. Field, *Corrosion* **2013**, *17*, 571t.
299. C. Wang, F. Jiang, F. Wang, *Corrosion* **2004**, *60*, 237–243.
300. N. Birbilis, R. G. Buchheit, D. L. Ho, M. Forsyth, *Electrochem. Solid-State Lett.* **2005**, *8*, C180.
301. B. R. W. Hinton, *J. Alloys Compd.* **1992**, *180*, 15.
302. S.-H. Zhang, G. Kong, J.-T. Lu, C.-S. Che, L.-Y. Liu, *Surf. Coatings Technol.* **2014**, *259*, 654.
303. P. Visser, Y. Liu, H. Terryn, J. M. C. Mol, *J. Coatings Technol. Res.* **2016**, *13*, 557.
304. P. Visser, Y. Liu, X. Zhou, T. Hashimoto, G. E. Thompson, S. B. Lyon, L. G. J. Van Der Ven, A. J. M. C. Mol, H. A. Terryn, *Faraday Discuss.* **2015**, *180*, 511.
305. X.-B.o Chen, X. Zhou, T. B. Abbott, M. A. Easton, N. Birbilis, *Surf. Coatings Technol.* **2013**, *217*, 147.
306. L. Jiang, M. Wolpers, P. Volovitch, K. Ogle, *Corros. Sci.* **2012**, *55*, 76.
307. Q. Liu, T. L. Dzwiniel, K. Z. Pupek, Z. Zhang, *J. Electrochem. Soc.* **2019**, *166*, A3959.
308. C. F. Glover, C. Richards, J. Baker, G. Williams, H. N. Mcmurray, *Corros. Sci.* **2017**, *114*, 169.
309. S. Pourhashem, M. R. Vaezi, A. Rashidi, M. R. Bagherzadeh, *Corros. Sci.* **2017**, *115*, 78.
310. D. D. Macdonald, S. R. Biaggio, H. Song, *J. Electrochem. Soc.* **1992**, *139*, 170.
311. E. J. W. Verwey, *Physica* **1935**, *2*, 1059.

How to cite this article: S. A. Skaanvik, S. M. Gateman, *Electrochem Sci Adv* **2023**, e2300014. https://doi.org/10.1002/elsa.202300014